TUNABLE PHOTOPUMPING IN DEVELOPING ZnSe LASERS

By

YU GUAN

A DISSERTATION PRESENTED TO THE GRADUATE SCHOOL
OF THE UNIVERSITY OF FLORIDA IN PARTIAL FULFILLMENT
OF THE REQUIREMENTS FOR THE DEGREE OF
DOCTOR OF PHILOSOPHY

UNIVERSITY OF FLORIDA

1991

TO MY PARENTS,

JIERU GUAN AND ZEYAN GAO

ACKNOWLEDGMENT

I wish to express my sincere gratitude to Dr. Peter S. Zory, my advisor, for leading the way. His commitment, enthusiasm and expertise have made possible all these accomplishments in the lab we built from scratch.

I am very grateful to Dr. Charles A. Zmudzinski for his valuable advice and constant assistance, on both theoretical and technical issues. I also thank Dr. Sheng S. Li, Dr. Ramakant Srivastava and Dr. C. K. Peng for the benefit I have received from their classes and their critiques at my oral examinations.

I would like to thank Dr. Robert M. Park for providing the MBE grown ZnSe materials and the advice I received from him. I also thank Dr. Jae Kim and Dr. Balu Pathengy for providing the MOCVD grown ZnSe, annealing equipment and microphotographic facilities.

I wish to thank Mr. Johan Sandell and A. Deneuville for their help in the optical absorption measurement of ZnSe.

My appreciations also extend to Dr. Jae Yoo, Mr. Youngsoh Park, Dr. Yaowang Lin, Ms. Suzhen Zhu and Ms. Yun Wang for processing and characterizing the materials, to Mr. Allan Herrlinger, Mr. James Chamblee and Mr. Jim Hales for their assistance in the machine shop and the clean room, to Mr. Hsing Chien Cheng and Mr. Horngjye Luo for their help on software and Mr. Gab Lim, Mr. Douglas Hudson and Mr. Robert McClain for their support and friendship.

TABLE OF CONTENTS

Page

ACKNOWLEDGMENTS....iii

ABSTRACT....vi

CHAPTER

1. INTRODUCTION....1

2. EXPERIMENT....7

2.1. Tunable Photopump....7

2.1.1. Sample Preparation....7

2.1.2. Optics and Electronics....12

2.2. Beam Characteristics....15

2.3. Optical Absorption of ZnSe....17

3. DISCUSSION....25

3.1. Optical Gain....25

3.2. Absorption Saturation....33

3.3. Bulk ZnSe lasers....41

3.3.1. Pump Wavelength Dependence of the Laser Performance....44

3.3.2. Near and Far Fields....48

3.3.3. Gain Guiding Model....53

3.3.4. Comparison with Bulk GaAs Lasers....60

3.4. Epitaxial ZnSe Lasers....64

3.4.1. Pump Wavelength Dependence of the Laser Performance....66

3.4.2. Continuity Equation Model....73

3.4.3. Epilayer Thickness Dependence of the Laser Performance....84

3.4.4. Comparison with GaAs lasers and Bulk ZnSe lasers....88

3.4.5. Leaky Waveguide Model....88

4. SUMMARY AND PROPOSALS.....94
REFERENCES.....104
BIOGRAPHICAL SKETCH.....109

Abstract of Dissertation Presented to the Graduate School of the University of Florida in Partial Fulfillment of the Requirements for the Degree of Doctor of Philosophy

TUNABLE PHOTOPUMPING IN DEVELOPING ZnSe LASERS

By

Yu Guan

May, 1991

Chairman: Peter S. Zory
Major Department: Electrical Engineering

Experimental and theoretical results on developing blue light emitting ZnSe lasers using tunable photopumping are presented. The work started with feasibility studies of lasing in ZnSe material and the demonstration of room temperature laser operation in photopumped ZnSe. It then extended to the analysis and modeling of the pump wavelength dependence of the laser performance. A similar study was also done for photopumped lasers made of GaAs, the most commonly used diode laser material. The results were compared with that of the ZnSe lasers in order to assess the potential of fabricating ZnSe based diode lasers

By selecting appropriate pump wavelengths, first time room temperature laser oscillation in bulk ZnSe was accomplished. The

differential quantum efficiency η_d of such lasers was found to be a strong function of pump wavelength λ_p. Such dependence is interpreted by using gain guiding theory and by analyzing data on beam characteristics, which is believed to be the first for photopumped lasers. The results are useful for understanding carrier and photon confinement in such lasers and for designing potential ZnSe diode lasers. It was also discovered that the saturation of optical absorption significantly affects η_d. Utilizing the tunable photopump system, this effect was measured and compared with the theory.

Photopumped epitaxial ZnSe lasers were fabricated from MBE and MOCVD grown thin film ZnSe on GaAs substrates. The relation of η_d vs. λ_p is once again studied and compared with that of bulk ZnSe and GaAs lasers. It is shown that the optical loss associated with the TE_0-like mode of the antiwaveguide thin film structure can be quite low, in contrary to what might be expected. Such antiguide structures thus have the potential of being used for fabricating superluminescent blue edge light emitting diodes (ELEDs), and ELED arrays.

It is demonstrated by this work that the tunable photopump is a convenient and effective tool for developing new diode laser materials and structures.

CHAPTER 1
INTRODUCTION

The motivation for developing ZnSe diode lasers mainly comes from the demand for efficient and low cost coherent light sources in the blue part of visible wavelengths. Having shorter wavelength and higher photon energy, blue light is more valuable for optical data storage and laser printing than the infrared light being used today [Camm87]. This is because blue light can be focused into a smaller spot than the infrared so that three to four times more information can be stored on the same area of storage medium [Feit88]. Higher photon energy carried by blue light enables us to select from a larger variety of materials for the storage medium [Reyn89]. In addition, for color display uses, either flat panels or projection TVs, blue light is a fundamental color element [Guns88]. For underwater applications, blue light is of particular interest because it is subject to minimum attenuation in water among electromagnetic waves of all wavelengths [Chun90].

Blue coherent light can be generated via four general approaches: (1) gas lasers or liquid (dye) lasers, (2) frequency upconversion from solid state lasers, (3) frequency upconversion from infrared diode lasers, and (4) blue diode lasers. Gas lasers, dye lasers and solid state lasers do generate high power blue laser beams. However, they are all too bulky, heavy and costly for most

applications. Their power efficiency is low (usually much less than 1%) and they require either separate high voltage power supplies or a second laser for operation. A nonlinear crystal used along with a regular infrared diode laser does significantly reduce the size and weight. Unfortunately, the conversion efficiency and the absolute output power provided by today's existing crystals are very limited [Dixo90]. Furthermore, although the size of the most recently reported nonlinear blue converter has been made as small as a packaged diode laser [Lent90], it is not optimistic that much further reduction in size can be achieved. This means that it is unlikely for such devices to be used for OEICs (OptoElectronic Integrated Circuits) or flat panel displays, where sub-millimeter size light emitters are essential. It is also difficult for this type of device to be used for multi-track, individually addressable reading or writing heads for optical storage, which have particularly high access speed and data density [Gree89]. On the other hand, semiconductor diode lasers do not have the above shortcomings which are inherent to other types of blue lasers. Diode lasers and light emitters are thus believed to be the most promising coherent blue light sources with the greatest market potential.

The main technical barrier for making a blue semiconductor laser or an LED (Light Emitting Diode) is to find the right semiconductor materials and to dope them appropriately. To fabricate a diode laser, the semiconductor material being used must have direct energy bandgap [Dumk 62] and must be doped into both p and n types (Figure 1-1). In addition, cladding layers made of materials of larger energy bandgaps and smaller refractive indices

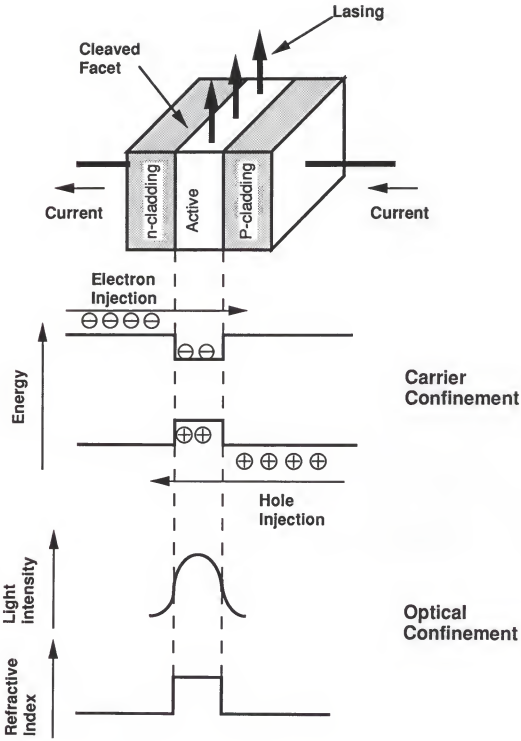

Fig. 1-1. A typical diode laser

are also needed for confining the carriers and the laser mode, which is essential for the proper operation of the diode laser [Case78]. In the last two decades, many II-VI compounds have been studied by photopump for the possibility of making blue and green lasers. Among them, there are ZnTe, ZnSSe, ZnSe, ZnMnSe, CdSSe, CdS, etc. [John71, Byls85, Glas88, Guns88, Suem89]. Those experiments were all done with fixed pump wavelength and at temperatures below 200K. Room temperature photopumped laser action has not be demonstrated at blue wavelengths for these materials. On the other hand, current injection blue LEDs have been fabricated by using SiC [Cons91] and ZnSe [Park90b, Ren90, Akim90]. Confinement structures need to be built to further develop them into laser diodes. ZnSe blue emission from Schottky diodes [Alle73] and metal-insulator-semiconductor (MIS) structures [Jain88] have also been proposed. In this work, it is shown that ZnSe is one of the most promising materials for fabricating blue diode lasers. This is done by presenting the first results on room temperature operation of photopumped bulk and epitaxial ZnSe lasers. Another goal of this work is to demonstrate that tunable photopump, an approach seldom used by others, is a useful and convenient tool for studying new diode laser materials and structures.

Experimental details will be given in Chapter 2. The main part of this chapter is a description of the tunable photopump set-up and technique. Fabrication of both bulk and epitaxial ZnSe laser samples as well as the optical and electronic systems for data acquisition will be described. In order to establish appropriate models for interpreting the tunable photopump data, experiments were also

done to study the beam characteristics of such lasers and the optical absorption properties of ZnSe. Corresponding apparatus is illustrated in this chapter.

In Chapter 3, major results from tunable photopump experiments are discussed and a few theoretical models presented. The optical gain of ZnSe as a function of pump intensity is estimated by studying the spectral narrowing of its photoluminescence (PL). Optical absorption coefficient as a function of light intensity is calculated and used for interpreting the laser performance data. By analyzing the beam characteristics of photopumped bulk ZnSe lasers, the pump wavelength dependence of differential quantum efficiency η_d and threshold pump intensity I_{th} are calculated and compared with experimental data. The results show the importance of selecting pump wavelengths for achieving room temperature lasing in ZnSe. The results are also compared with data from a photopumped bulk GaAs laser to demonstrate that ZnSe can be as good a material as GaAs, a standard diode laser medium, for making lasers. Photopumped lasers made of thin film ZnSe epitaxially grown on GaAs substrates were also studied to demonstrate the feasibility of fabricating a ZnSe diode laser. A model based on the continuity equation is established for estimating the carrier and optical field profiles in such a structure. Once again, η_d and I_{th} are calculated as functions of pump wavelengths and compared with the experimental results. These dependences are also compared with those of photopumped bulk ZnSe lasers to show the optical confining ability of these epitaxial ZnSe structures. Leaky waveguide theory is employed for interpreting the confinement, which shows that the waveguide

loss of such a structure is much less than usually expected, in spite of an undesired negative refractive index step. It is therefore hoped that the structure would have device applications.

Finally, in Chapter 4, some preliminary results on fabricating ZnSe edge light emitting diodes (ELEDs) and array ELEDs are presented after a summary of previous chapters. Some proposals on designing anti-guide double heterojunction diode lasers are also made in this chapter.

CHAPTER 2
EXPERIMENT

2.1 Tunable Photopump

2.1.1. Sample Preparation

Three types of ZnSe samples were used for making photopumped lasers. They are single crystal bulk ZnSe, thin film ZnSe grown by molecular beam epitaxy (MBE) on GaAs substrates and thin film ZnSe grown by metal-organic chemical vapor deposition (MOCVD) on GaAs substrates. All of the samples were not intentionally doped.

The bulk ZnSe samples were melt-grown by Eagle Pitcher Company. They came in the shape of 0.9 mm thick, 5 mm × 5 mm square wafers, as shown in Fig. 2-1 (a). They were claimed to be (111) oriented single crystals with some twin structures. Both the top and the bottom sides had been mechanically polished. The edges were sawed to separate them from a bigger piece. To shape them into laser resonators illustrated in Fig. 2-1 (b), they must be thinned and cleaved. Thinning was done on one side of the wafer on a Lapmaster lapping machine with 9 μm diameter aluminium oxide powder. The other side remained intact and was to be photopumped (see Fig. 2-1 (b)). The thinned wafers were then cleaved into bars of 200 μm width. Since the wafer is a (111) oriented zincblende crystal,

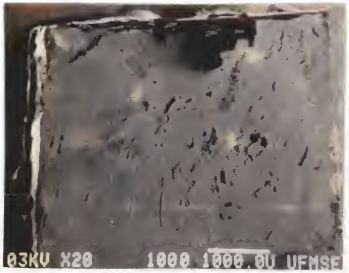

(a)

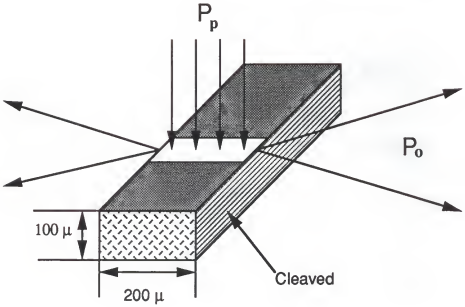

(b)

Fig. 2-1. Bulk ZnSe. (a) A single crystal wafer. (b) A cleaved resonator.

there is only one group of (110)-type planes perpendicular to the (111) surface, along which cleaving is possible. The wafers were not originally sawed along the cleavage direction. Test cleave had to be made to find the angle the cleavage direction makes with respect to one sawed edge. The wafers were then scribed on a scribing machine in the cleavage direction and cleaved into bar shaped resonators. The width of the bars (200 μm) is the cavity length of the resonators. As illustrated in Fig. 2-1 (b), once appropriate pump light is incident on the top side of the resonator, laser light will emit from both cleaved facets.

Both MBE and MOCVD grown thin film ZnSe were deposited on (100) oriented GaAs substrates and therefore the ZnSe is also (100) oriented. There is a slight lattice mismatch (0.25%) between ZnSe and GaAs [Guns89]. The MBE samples used for this work have 1μm thick epilayers. They were prepared by the Materials Science and Engineering Department of the University of Florida. Samples of various epilayer thickness (0.5 μm to 3.5 μm) were grown by MOCVD to study the laser performance as a function of epilayer thickness. MOCVD samples were prepared by the Chemical Engineering Department of the University of Florida. Cross section views of these samples are given in Fig. 2-2 (a). The wafers were processed in a way similar to that for the bulk wafers. Lapping and scribing were done on the substrate side. The optical geometry for the photopump experiment was also the same, as illustrated in Fig. 2-2 (b).

MBE, t = 1μm

MOCVD, t = 3.5μm

Fig. 2-2. Epitaxial ZnSe. (a) Picture showing ZnSe thin film on GaAs substrate.

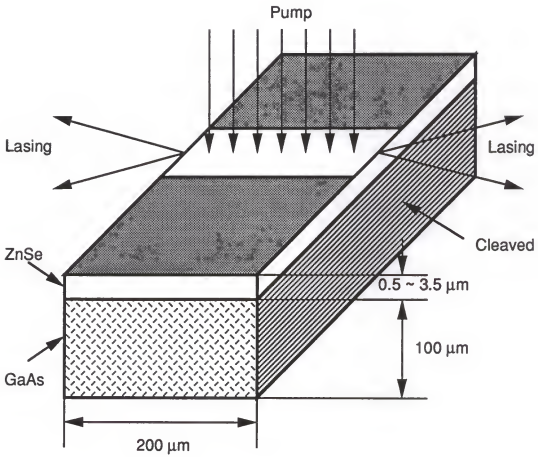

Fig. 2-2. Epetaxial ZnSe. (b)Illustration of a cleaved epitaxial ZnSe resonator.

2.1.2. Optics and Electronics

The entire tunable photopump experimental system is sketched in Fig. 2-3. A cleaved resonator, either made from a bulk or an epitaxial sample, was attached to its holder at one end such that the pumped region is free standing. At room temperature, it was pumped by a N_2 laser pumped tunable dye laser. The pulse width and repetition rate of the dye laser output were about 6 ns and 10 Hz, respectively. The pump light was attenuated to the desired intensity using a rotational neutral density filter with gradually changing optical density. It was then focused onto the surface of the ZnSe resonator with two crossed cylindrical lenses. A PIN photodiode, calibrated with respect to the power in the focused pump beam, including losses in the focusing optics, was used to record the pump power. The light emission from the ZnSe output facet was collected with a high power microscope objective lens and focused into a grating monochromator to measure the spectral characteristics of the ZnSe laser output.

The low duty cycle laser output pulses were processed by a boxcar averager to convert the peak magnitude of each pulse into a DC signal for the X-Y recorder. This process is illustrated in Fig 2-4. The laser output signal depicted in part (a) is the voltage output from the photomultiplier (PMT) attached to the monochromator. Its shape is not the same as the real time light signal because the time constants of the input circuits of the oscilloscope and the boxcar are too large to follow the short light pulses. Its peak magnitude V_o, on the other hand, is proportional to the peak power of the light signal. The boxcar generates a DC voltage V_o', which is proportional to the

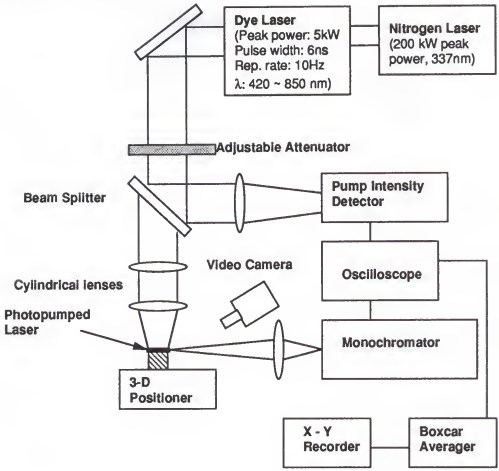

Fig. 2-3. Schematics of tunable photopump experiment.

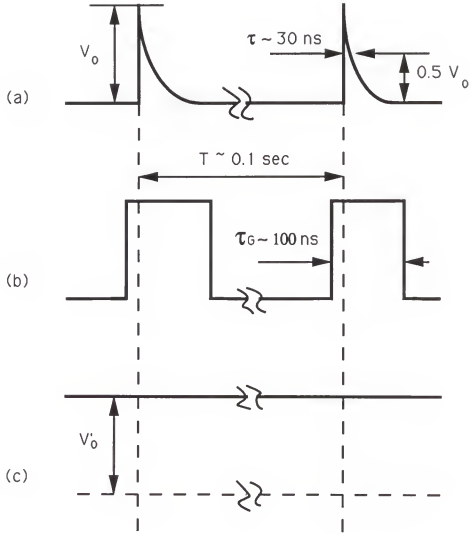

(a) Laser output signal
(b) Gate signal
(c) Peak magnitude of laser output

Fig. 2-4. Signal acquisition using a boxcar.

average input voltage during τ_G, the time duration when its electronic gate is open. By adjusting the system amplification, V_0' can be set equal to V_0. Gate width τ_G should be small enough to ensure sufficient signal to noise (S/N) ratio and large enough to accommodate the pulse jitter so that the input pulse will not fall outside the gate. A DC signal for the pump light intensity can be obtained in the same way.

To estimate the pump power density, the area of the pumped region needs to be measured. The pumped surface and an output facet of the resonator were monitored with a video system. Picture of the surface taken by the video camera was send to a video analyzer. The analyzer was able to scan either horizontally or vertically across the picture and to plot the intensity variation throughout the scan. Such plots are presented in Fig. 2-5. Plot (b) was made with the real sample in its place and the pump light on. Plot (a) was made with the sample replaced with a 200 μm wide slit. The vertical dimension of the pumped region can be calculated by comparing plot (a) and (b). Aspect ratio, scan speed and the angle the camera pointing at the resonator all need to be considered in the calculation. The calculated vertical size of pumped region from these two plots is about 175 μm and the pumped area is 175 μm × 200 μm = 3.5×10^{-4} cm^2.

2.2 Beam Characteristics

Near and far field pictures of these photopumped lasers were also taken. Since the pump wavelength was very close to the lasing wavelength and the pump intensity is two orders of magnitude larger than that of the laser light, some special measures had to be

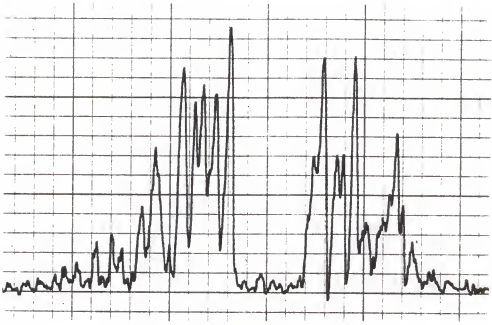

(a) Horizontal (Scale: 1div. = 50 μm)

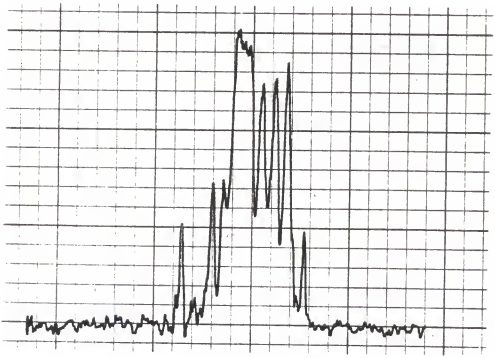

(b) Vertical (Scale: 1div. = 35 μm)

Fig. 2-5. Estimate of pumped area on the sample.

taken. As illustrated in Fig. 2-6 (a), for recording the near field profile, a "50 x" microscope objective of large numerical aperture (0.55) was used to collect as much laser light as possible. One or two Corion bandpass interference filters were inserted between the objective and the eyepiece to prevent pump light from entering the camera. According to the manufacturer, two such filters are able to attenuate the light of 460 nm by 40 db with respect to the 470 nm laser light. The optical system provides us with a magnification of about 1000 so that changes in the near field profile can easily be measured.

To take pictures of the far field, a thin diffusion screen was placed at a certain distance from the laser facet, as shown in Fig. 2-6 (b). The diffusion screen was made from a microscope cover glass by thinning it on a Lapmaster lapping machine so that it became a 30 μm thick ground glass. The interference filters were still needed for the same reason. Magnification of the optics is much smaller because the size of the far field patterns is much larger.

2.3. Optical Absorption of ZnSe

Since these ZnSe lasers were pumped at near-bandgap wavelengths, the variation of absorption of the pump light with wavelength is significant [Kitt76]. As it will be discussed later, the laser performance, including the threshold and the differential quantum efficiency, as well as the carrier and laser mode distributions, depend strongly on the change in optical absorption. Although there exist data on the optical absorption properties of ZnSe in the literature, they are for small signal situation only and seem to

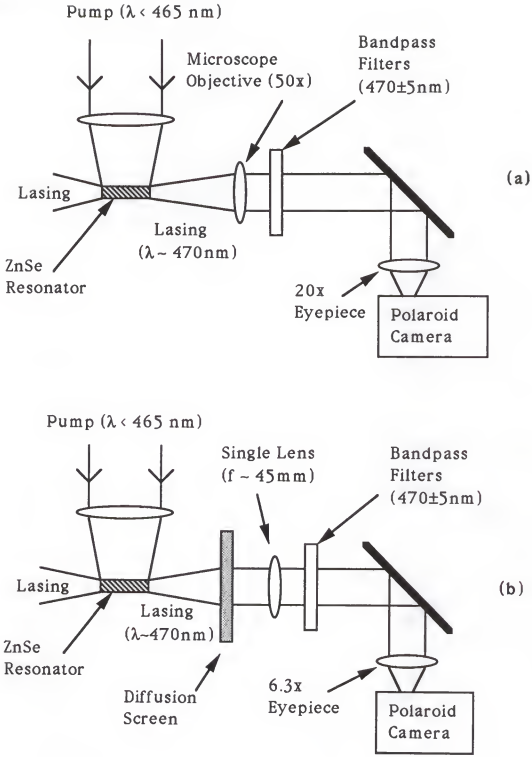

Fig. 2-6. Experimental set-ups for measuring (a) near field and (b) far field profiles.

be inconsistent [Avan61, Phil63, Wang81, Ando85, Ves85]. In order to establish an appropriate model and to properly understand the physical processes in these photopumped lasers, optical absorption measurements need to be made at the light intensity level at which the lasers operate and with exactly the same sample materials used for making these lasers.

The large variation of the absorption coefficient of ZnSe in the wavelength range of interest requires samples of different thicknesses for transmissivity measurements. A piece of bulk ZnSe wafer, which was originally 900 μm thick, was thinned to 35 μm. After thinning, the wafer was polished on a polishing machine using a nylon pad and 0.25 μm diamond paste. Bulk wafers with both sides polished were thus obtained in two thicknesses, 35 μm and 900 μm. For the epitaxial wafers, a window needed to be opened on the substrate to get an area of 2 μm thick free standing ZnSe. This was done by selective etching and is illustrated in Fig. 2-7. Photoresist was applied on the substrate side of the wafer. A round area of about 1 mm in diameter was exposed. The wafer was then attached epilayer side down to a glass plate with wax and etched with NH_4OH / H_2O_2 for about 20 minutes. Once the GaAs in the window area was gone, the sample was removed from the glass plate and transferred to a sample holder shown in Fig. 2-8 and Fig. 2-9. A dummy GaAs wafer with an etched window of the same size was meanwhile prepared to serve as the bare window for reference during the measurements.

For the small signal situation, the apparatus shown in Fig. 2-8 was sufficient and convenient for transmission measurements. The

(a)

(b)

(c)

Fig. 2-7. Illustration of the sample for absorption measurement. (a) Photoresist pattern on the area where the subatrate is to be etched. (b) Substrate halfway etched. (c) A window created on the substrate.

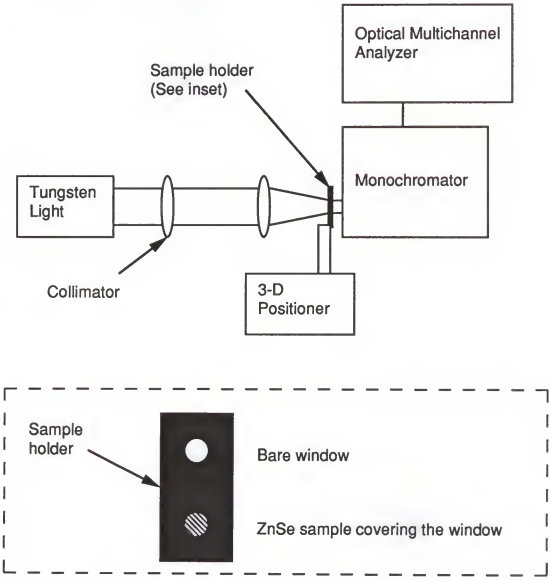

Fig. 2-8. Schematics of absorption measurement system for small signal situation.

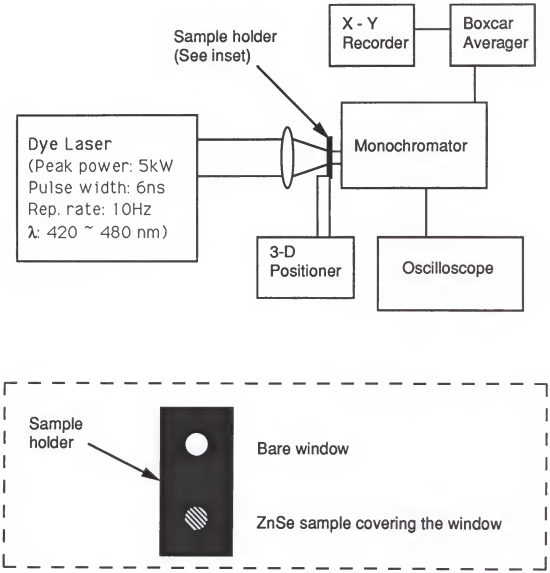

Fig. 2-9. Schematics of absorption measurement system for large signal situation.

tungsten light generated continuous spectrum throughout the wavelength range of interest. The transmission spectrum was obtained by dividing the spectrum recorded with the ZnSe sample covering the window by the spectrum recorded with the bare window. With known sample thickness and surface reflectivity, absorption spectrum was calculated from the transmission spectrum.

When the light intensity increases to the level of the pump intensities used for these lasers, the optical absorption of ZnSe may saturate and the transmission may increase significantly. To obtain data for this situation, the tungsten light in Fig. 2-8 was replaced by the same dye laser used for the tunable photopump. Since the dye laser output is pulsed, it needed to be converted to a DC signal with a boxcar averager. Figure 2-9 depicts the entire set-up. The absorption spectrum were obtained in basically the same manner as in the small signal case except that it was done point by point. In other words, absorption coefficient at only one particular wavelength could be obtained at a time because the spectral width of the dye laser output is so narrow. The monochromator scanned in the neighborhood of the dye laser wavelength. The transmissivity of ZnSe at this wavelength is therefore the ratio of the peak spectral height with the sample on to the peak spectral height with the bare window on. This process was repeated while the dye laser was tuned over the wavelength range of interest. Figure 2-10 shows 13 pairs of such scans. The upper and the lower peaks at each wavelength correspond to that with the bare window only and with the ZnSe sample on, respectively.

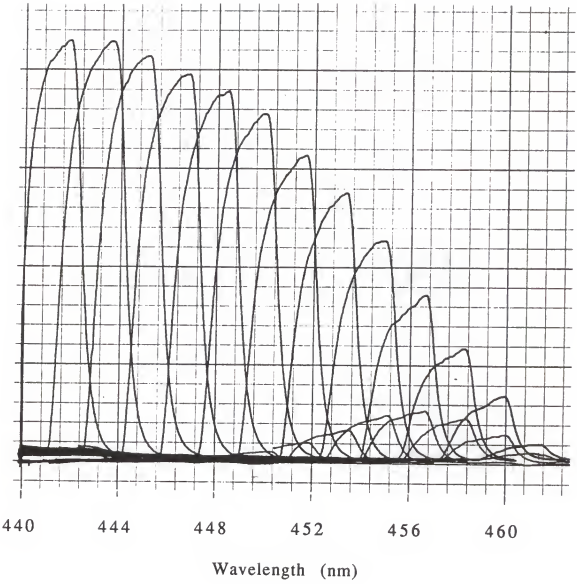

Fig. 2-10. Spectral curves for determining large signal α.

CHAPTER 3
DISCUSSION

3.1 Optical Gain

Optical gain is one of the key parameters to determine the feasibility and suitability for a material as a laser medium. Without shaping the material into a laser cavity, the sign of optical gain can usually be seen by looking for the spectral narrowing effect in the photoluminescence (PL) spectra of the material [Shak73]. In addition to optical gain, these spectra can also be expected to provide data on excitation intensity, wavelength and temperature required to obtain such a gain. This information is of fundamental importance in designing and operating a laser. Since the PL spectra can be obtained by using the tunable photopumping system shown in Fig. 2-3 with minimum changes, it is sensible to start the investigation by analyzing PL spectra.

The PL spectra of ZnSe shown in Fig. 3-1 were measured at room temperature with the experimental system illustrated in Fig. 2-3. The only difference is that the photopumped laser was replaced with a bulk ZnSe wafer with only one cleaved edge, which faces the monochromator. All other sides were uncleaved so that no resonator was formed and no optical oscillations occurred. The excitation intensity was varied by rotating the attenuator. The length of the

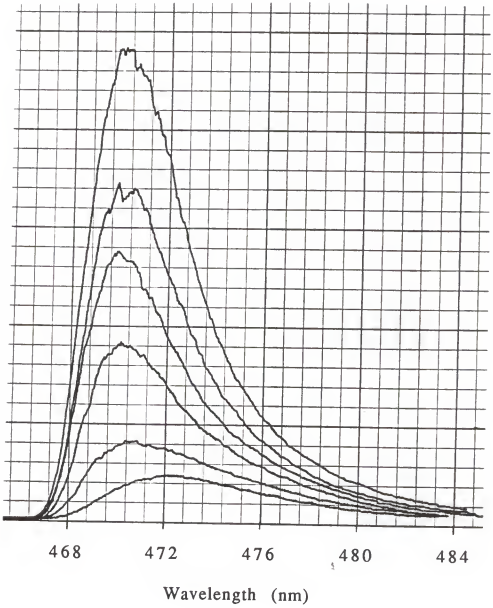

Fig. 3-1. Spectral narrowing effect in ZnSe (a) Spectra for various input power P_i at L = 550 μm. Corresponding P_i's (beginning from the top curve): 400 W, 350 W, 300 W, 260 W, 210 W, and 175 W.

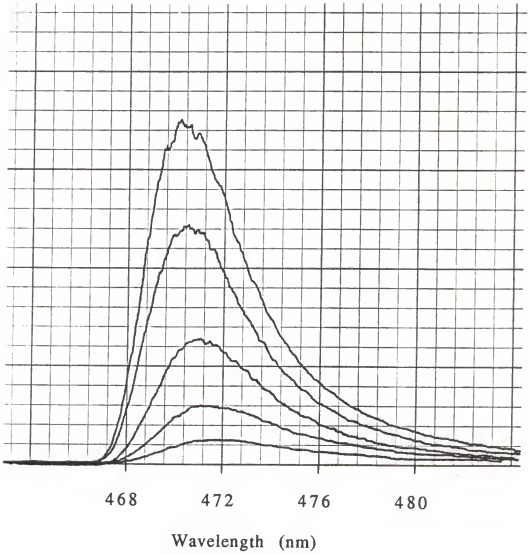

Fig. 3-1. Spectral narrowing effect in ZnSe (b) Spectra for various length of pumped section L at P_i = 350 W. Corresponding L's (beginning from the top curve): 550 μm, 450 μm, 350 μm, 250 μm, and 150 μm.

excited region was varied by blocking part of the input light using a razor blade placed right next to the sample wafer.

According to the theory concerning light-material interaction [Bakk77, Verd81], if the material has optical gain, the amplified spontaneous emission power P_o is related to the gain g_o (for small signal case) by

$$P_o(\nu) = \frac{h\nu A_{21} N_2}{g_o(\nu_o)} \{\exp[g_o(\nu)L] - 1\} \tag{3.1}$$

and

$$g_o(\nu) = g_o(\nu_o) \frac{(\Delta\nu / 2)^2}{(\nu - \nu_o)^2 + (\Delta\nu / 2)^2}, \tag{3.2}$$

where ν is the light frequency, ν_o is the peak gain frequency, h and A_{21} are the Plank constant and the Einstein coefficient, respectively, and N_2 is the upper level population of ZnSe. It is noticed from Eq. (3.2) that the gain is a function of frequency and is assumed to have Lorentz shape. The gain linewidth $\Delta\nu$ is about the same as the PL linewidth under very low excitation level (when there is virtually no optical gain).

To calculate $g_o(\nu_o)$ from PL linewidths, in the first order approximation, it is further assumed that N_2 and $g_o(\nu_o)$ are both proportional to I_i in the small signal situation. Therefore,

$$g_o(\nu_o) = \beta I_i - \alpha_o, \tag{3.3}$$

and

$$P_o(\nu) = C_1 \{ C_2 \exp[\frac{(\Delta\nu / 2)^2}{(\nu - \nu_o)^2 + (\Delta\nu / 2)^2} \beta I_i L] - 1\}, \tag{3.4}$$

where I_i is excitation intensity, α_o is the small signal absorption coefficient, C_1, C_2 and β are constants independent of I_i and ν within $\Delta\nu$. Define the full width at half maximum (FWHM) of the PL spectrum $\Delta\nu_1$ as the range in which $P_o(\nu)$ is larger than one half of $P_o(\nu_o)$, i.e. $P_o(\nu_1) = 0.5P_o(\nu_o)$ and $\Delta\nu_1 = 2|\nu_1 - \nu_o|$. When the gain and the length of the excited region are sufficiently large, the second term in (3.4) can be ignored and β can be related to $\Delta\nu_1$ by

$$\frac{1}{(\Delta\nu_1)^2} = \frac{1}{\ln 2} \times \frac{1}{(\Delta\nu)^2} \beta I_i L. \tag{3.5}$$

The line width $\Delta\lambda$ of the low level excitation PL spectra was found to be about 16 nm for bulk ZnSe, from which $\Delta\nu$ can be calculated. Corresponding $(\Delta\nu_1)^{-2}$ vs. I_i and $(\Delta\nu_1)^{-2}$ vs. L relations are obtained using the data in Fig. 3-1 and are illustrated in Fig. 3-2 and Fig. 3-3. By curve fitting, β can be calculated from these data and Eq. (3.5). Consequently, peak small signal gain $g_o(\nu_o)$ as a function of excitation intensity I_i is obtained from Eq. (3.3). The result is presented in Fig. 3-4. Note that P_i has been converted to I_i by $I_i = P_i / A$, where A is the surface area of the sample being excited and has been given in Sec. 2.1.

The resulting gain values of ZnSe are comparable to several other semiconductor laser media [Thom82, Case78, Agra86]. It indicates that when the sample is optically excited at the level shown at the high end of Fig. 3-4, the gain can be expected to overcome the losses and laser oscillation should start once an optical resonator is properly constructed. Of course, when the sample is pumped to near its lasing threshold, the optical gain will saturate and deviate from

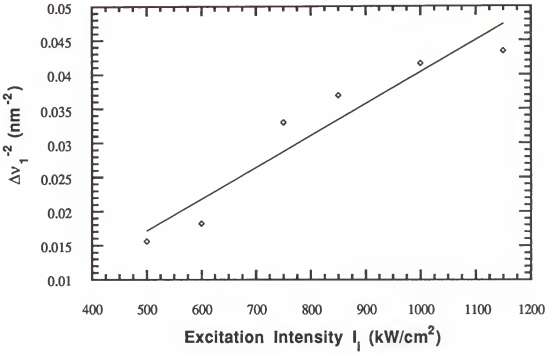

Fig. 3-2. $\Delta\nu_1^{-2}$ vs. I_i for ZnSe PL at L = 550 μm.

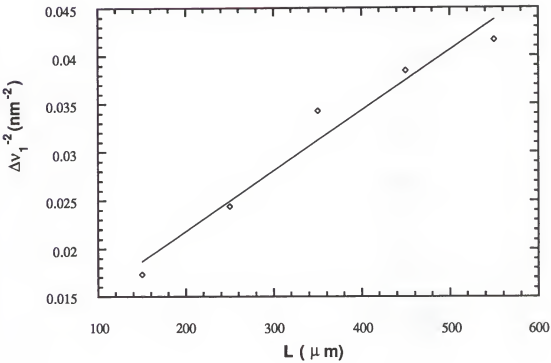

Fig. 3-3. $\Delta\nu_1^{-2}$ vs. L for ZnSe PL at P_i = 350 W.

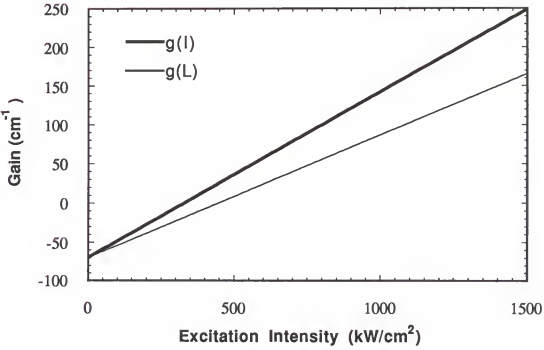

g(I): Gain calculated from Δv_1^{-2} vs. I_i
g(L): Gain calculated from Δv_1^{-2} vs. L.

Fig. 3-4. Estimate of optical gain of ZnSe.

this calculation. A laser model will then be used to discuss that situation.

3.2. Absorption Saturation

Since ZnSe is a direct bandgap material, it is expected to have a vary sharp optical absorption edge near its energy band gap, which corresponds to about 480 nm in wavelength [Era70]. The small signal absorption coefficient α_o was measured by using the apparatus and samples described in Sec. 2.3. Resulting absorption spectrum in the neighborhood of the energy bandgap of ZnSe is given in Fig. 3-5. It was calculated under the assumption that α_o is independent of light intensity. Suppose I_i and I_o are the input and transmitted light intensities (intensities of the light passing the window without and with a sample covering it, respectively), t is the sample thickness and R is the surface optical reflectivity of ZnSe, then for a homogeneous material

$$I_o = I_i\ (1 - R)^2 \exp(-\alpha_o t). \tag{3.6}$$

Therefore,

$$\alpha_o = -\frac{1}{t}\ln\left(\frac{I_o}{I_i}\right) + \frac{2}{t}\ln(1 - R). \tag{3.7}$$

Since R is known to be about 17% in this wavelength range [Phil63], α_o vs. wavelength λ can be obtained from experimental data on t and I_o/I_i vs. λ. Note that the experimental error increases significantly when I_o/I_i is close to zero or one. This is why each curve in Fig. 3-5 is not considered accurate near its ends and why samples of various

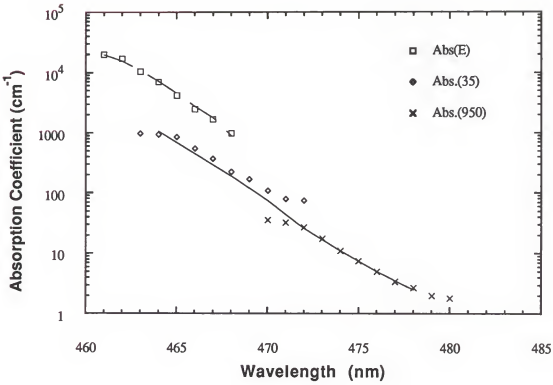

Abs. (35): Data from t = 35 μm bulk sample
Abs. (950): Data from t = 950 μm bulk sample
Abs. (E): Data from t = 2 μm epitaxial sample
———— : Fitting curve for bulk sample
— — : Fitting curve for epitaxial sample

Fig. 3-5. Absorption coefficient curves for ZnSe samples (at long wavelengths).

t's were used. The two fitting curves are the approximate α_o vs. λ for epitaxial and bulk ZnSe.

When I_i is sufficiently large, the optical absorption will no longer be a function of λ only, it also depends on the light intensity. Such phenomena is known as absorption saturation [Shea77]. In this experiment, when I_i approached the level of the threshold of these photopumped lasers (~300 kW/cm^2), the effective absorption coefficient α vs. λ was found like that shown in Fig. 3-6. Such an α is so defined that the light intensity decays to 1/e of I_i after traveling a distance of $1/\alpha$ in ZnSe. Small signal α_o vs. λ curve (measured on the same set-up at I_i ~ 20 kW/cm^2) is also plotted in Fig. 3-6 for comparison. From these two curves, the saturation light intensity I_s of ZnSe can be estimated. Usually, I_s is defined by [Verd81]

$$\frac{dI(\nu,x)}{dx} = \frac{\alpha_o\, I(\nu,x)}{1 + (I(\nu,x)\,/\,I_s)\,\gamma(\nu)}, \tag{3.8}$$

where x is the distance the light travels in the ZnSe material, $I(\nu,x)$ is the light intensity and $\gamma(\nu)$ is the lineshape function. $I(\nu_0,x)$ can thus be calculated by solving Eq. (3.8) numerically and the result is given in Fig. 3-7 for three different I_i levels ($I_i(\nu) = I(\nu,0)$). It has been assumed that $I(\nu)$ has Lorentz lineshape, i.e.

$$\gamma(\nu) = \frac{(\Delta\nu\,/\,2)^2}{(\Delta\nu\,/\,2)^2 + (\nu - \nu_o)^2}. \tag{3.9}$$

It can be seen that the $I(\nu_o,x)$ vs. x curve is more linearized as $I_i = I(\nu_0,0)$ becomes larger and larger in comparison to I_s. Meanwhile, α gets smaller. As λ changes, Eq. (3.8) also predicts changes in $I(\nu,x)$ vs. λ and α vs. λ. Since $I_s(\nu)$ has inverse cubic dependence on λ [Verd81],

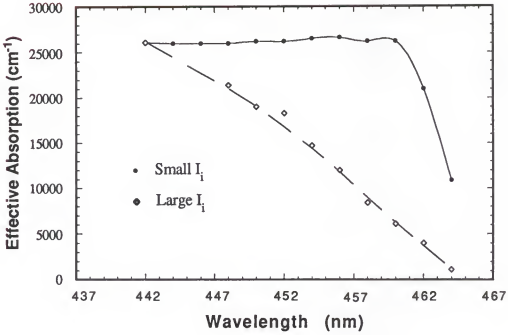

Fig. 3-6. Absorption coefficient curve for epitaxial ZnSe samples (at short wavelengths).

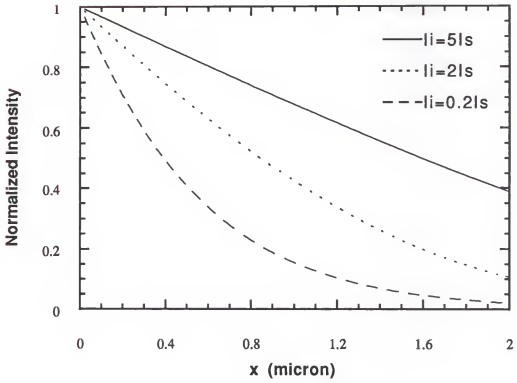

Fig. 3-7. $I_p(x)$ curves for small and big signals.

$$I_s(\nu) = \frac{4\pi^2 hc\Delta\nu}{\lambda^3 \tau_2 A_{21}}, \tag{3.10}$$

it does not change significantly in the wavelength range shown in Fig. 3-6 and the variation in large signal α mainly comes from the change in $\gamma(\nu)$. In Eq. (3.10), τ_2 is the upper level lifetime and c is the speed of light in vacuum. As a matter of fact, α_o, ν_o and $\Delta\nu$ are all known for these ZnSe samples (ν_o and $\Delta\nu$ are easily obtained from λ_o = 464 nm and $\Delta\lambda$ = 16 nm, see Sec. 3.1). The α vs. λ relation was thus calculated using Eq. (3.7) through Eq. (3.9) and compared with the experimental data, as shown in Fig. 3-8. Meanwhile, $I_s(\nu)$ of ZnSe was estimated to be about 100 kW/cm^2. This is believed to be in a reasonable range although no other data on this parameter of ZnSe has been reported so far.

Finally, it is noted that the small signal absorption coefficient α_o of epitaxial ZnSe measured by the two methods (shown in Fig. 2-8 and Fig. 2-9) is consistent. In Fig. 3-9, α_o is plotted as a function of the photon energy E and compared with optical absorption theory [Kitt76]. The fitting curve can be expressed by an equation

$$\alpha_o = 2.39 \times 10^5 \, [\, (E - 2.60)^{1/2} - (0.053)^{1/2}], \tag{3.11}$$

where α_o is in cm^{-1} and E is in electron volts. For high purity, direct band gap semiconductor material, such relation is of the form [Kitt76]

$$\alpha_o = K\,(E - E_g)^{1/2}, \tag{3.12}$$

where E_g is the bandgap energy and K is a constant independent of E. The discrepancy is believed to come mainly from the unknown dopants existing in ZnSe.

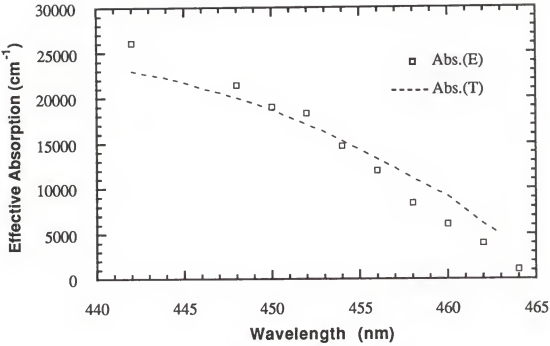

Abs. (E): Experimental
Abs. (T): Theoretical

Fig. 3-8. Effective optical absorption coefficient of epitaxial ZnSe (large signal)

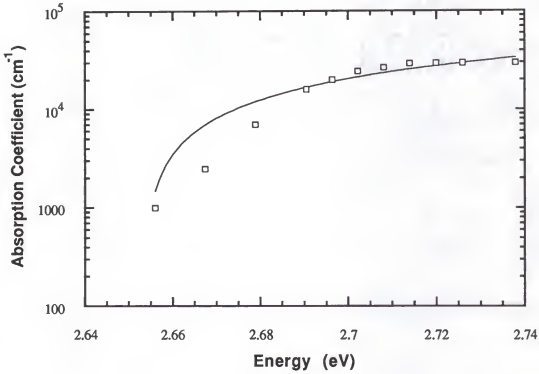

Squares: Experimental
Line: Theoretical

Fig. 3-9. Optical absorption coefficient of epitaxial ZnSe (small signal)

3.3. Bulk ZnSe Lasers

It has been established in the last two sections that once the ZnSe material is pumped by photons of appropriate wavelength, significant amount of pump energy will be absorbed by ZnSe and the optical gain induced may overcome the optical loss. If the ZnSe material has been shaped into appropriate optical resonator, a sharp laser spectral line is expected to emerge from the PL spectrum shown in Fig. 3-1. This was indeed observed when a bulk ZnSe resonator shown in Fig. 2-1 was photopumped at 457 nm at room temperature. Corresponding spectra are presented in Fig. 3-10, clearly indicating laser oscillations. The pump wavelength λ_p turned out to be critical for achieving laser action. As a matter of fact, the first attempt to operate these ZnSe lasers with direct nitrogen laser pump (λ_p = 337 nm) was a failure. There have been several other reports on nitrogen laser pumped bulk and superlattice epitaxial ZnSe lasers, none of them lased at room temperature [Sumu89, Cata82, Byls85]. Room temperature lasing was only achieved when the pump photon energy was tuned close to the bandgap energy of ZnSe, which corresponds to about 480 nm at room temperature. In addition, the laser output power also depends strongly on λ_p. It is much smaller at λ_p = 451 nm than at λ_p = 457 nm for the same pump intensity I_p [Zmud90]. In order to understand the λ_p dependence of the laser performance, the threshold pump intensity I_{th} and the differential quantum efficiency η_d are first studied.

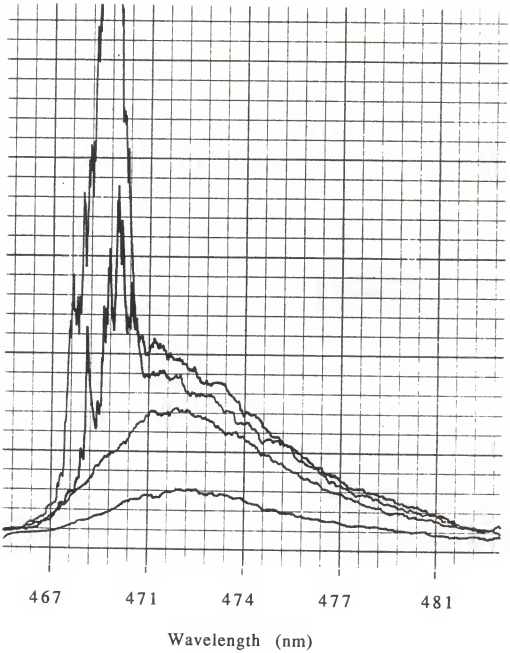

Fig. 3-10. Lasing spectra of bulk ZnSe, (a) just above threshold.

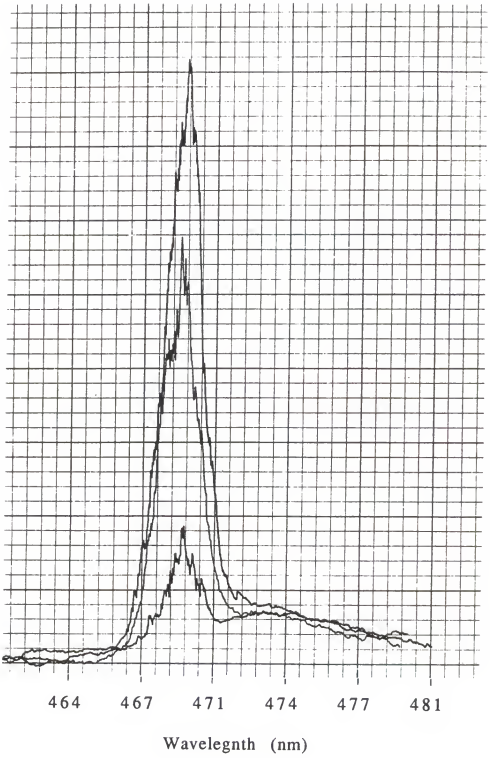

Fig. 3-10. Lasing spectra of bulk ZnSe, (b) well above threshold.

3.3.1. Pump Wavelength Dependence of the Laser Performance

Both η_d and I_{th} can be calculated from the P_o vs. I_p curve shown in Fig 3-11, where P_o is the laser output power from one facet. The threshold pump power P_{th} is defined as the P_p value at which the onset of laser oscillation occurs, i.e. where P_o takes off. The threshold pump intensity I_{th} is then determined by dividing P_{th} by the area of the focused pump beam on the ZnSe, i.e. $I_{th} = P_{th} / (W \times L)$. The measurement of W and L, which are the width and the length of the pumped region, has been described in Sec. 2.1.2. It can be seen in Fig. 3-11 that P_o depends on I_p linearly in most part of the $I_p > I_{th}$ range. It is sufficiently accurate, therefore, to assume that P_o vs. I_p follows a straight line as shown in Fig. 3-11 when $P_p > P_{th}$ and define η_d as

$$\eta_d \equiv \eta_i \, \eta_o \equiv \left[\frac{\lambda_o}{\lambda_p} \frac{P_G}{P_p - P_{th}} \right] \left[\frac{P_o}{P_G} \right], \tag{3.13}$$

where the first bracketed symbol, η_i, is the internal quantum efficiency, the second, η_o, is the output efficiency, P_G is the average laser power generated during each pump pulse and P_o and P_p are on the fitting line shown in Fig. 3-11. Therefore, η_d is independent of P_p. It can be seen from Eq. (3.13) that η_i is the ratio by which the above threshold pump photons are converted to laser photons. The output efficiency η_o can be expressed by [Wagn88]

$$\eta_o = \frac{\ln (1 / R_o)}{2L\alpha_i + 2\ln(1/ R_o)}, \tag{3.14}$$

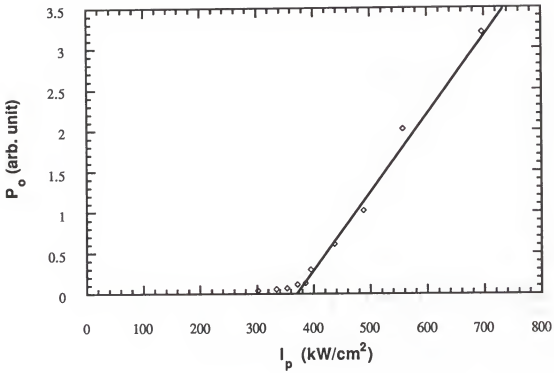

Fig. 3-11. P_o vs. I_p curve for a bulk ZnSe laser.

where R_o is the power reflectivity of the output facet, L is the resonator length and α_i is the internal loss coefficient. Both η_d vs. λ_p and I_{th} vs. λ_p are plotted in Fig. 3-12.

It is immediately known from Fig. 3-12 that there exists an optimum $\lambda_p \approx 461$ nm, where η_d is the highest and I_{th} is the lowest. It is also seen that η_d drops significantly as λ_p deviates from its optimum value. This is why such lasers do not operate at room temperature when pumped with $\lambda_p < 445$ nm, including the nitrogen laser wavelength (337nm). To understand the behavior of η_d, Eq. (3.13) and (3.14) need to be studied again.

In Eq. (3.14), R_o obviously does not have strong λ_p dependence. The most important mechanisms giving rise to α_i in these lasers are free carrier absorption, scattering and waveguide losses. The first two types of loss are usually under 20 cm^{-1} for semiconductor materials of good quality [Wagn88]. The waveguide loss, which results from the lack of an index waveguide structure in these lasers, is expected to be much higher than the first two but not to have significant change in the small λ_p range shown in Fig. 3-12. Therefore α_i and, consequently, η_o only depend weakly on λ_p. The strong dependence of η_d on λ_p in the figure must be due primarily to the dependence of η_i on λ_p. Since η_i is determined by the yield of laser photons, it is expected to depend strongly on the fractions of the laser mode in the gain and the loss regions. In other words, η_i depends on the laser mode profile and the gain profile in these lasers at various λ_p's.

The laser mode profile can be obtained directly from near field measurement. It is difficult, however, to measure the gain/loss

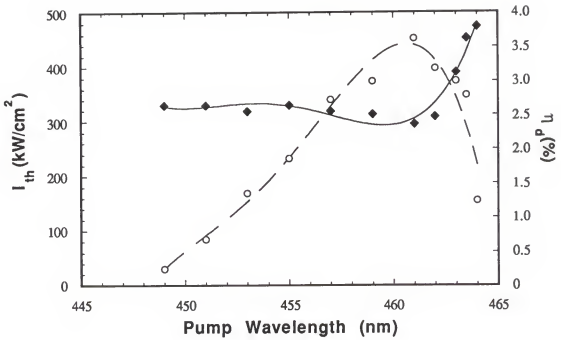

Fig. 3-12. η_d and I_{th} vs. λ_p for a bulk ZnSe laser.

profile directly. In the next section, a unique method of calculating the gain/loss profile by analyzing the near field and far field data is presented. The results can be used for a semi-quantitative estimate of the η_d vs. λ_p relation and for verifying the above theory.

3.3.2. Near and Far Fields

Near field pictures taken at short and long ends of the λ_p range in Fig 3-12 are presented in Fig 3-13. It can be seen that the field spreads more at longer λ_p. Exact near field profiles were plotted as described in Sec. 2.2. A typical profile is shown in Fig. 3-14.

Since the electric field (E) component of the far field is the Fourier transform of the near field E [Hech79], the far field profile is determined by both the magnitude and the phase variations of the near field E. As a result, a single-lobe near field may give rise to a double-lobe far field [Ster82], as shown in Fig. 3-15. By looking at the shape and size of the far field pattern, it can also be known from the Fourier transform theory that the near field is composed of a string of light emitting elements of approximately 3 μm $\times$ 3 μm in size. A plot of a typical far field profile is given in Fig. 3-16.

The fact that a single-lobe near field results in a double-lobe far field reveals that the equiphase front of the near field is curved rather than flat. A curved equiphase front is an evidence of gain guiding, an effect by which the laser photons are confined in the gain region even though there is no index guide [Asbe79]. The gain guiding effect is further evidenced by the beam waist recession effect [Cook74], in which the near field pattern appears to be located a certain distance behind the emitting facet. The amount of recession

Fig. 3-13. Near field pictures of a bulk ZnSe laser. (a) λ_p = 453 nm. (b) λ_p = 461 nm.

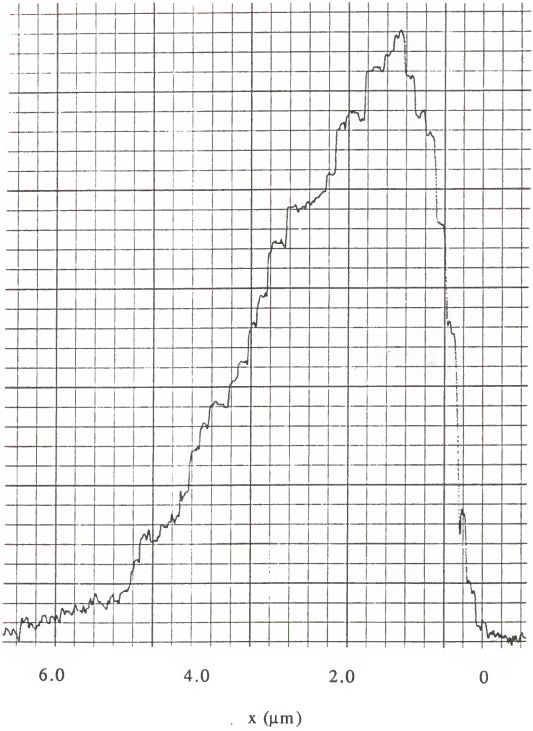

Fig. 3-14. Near field profile of a bulk ZnSe laser.

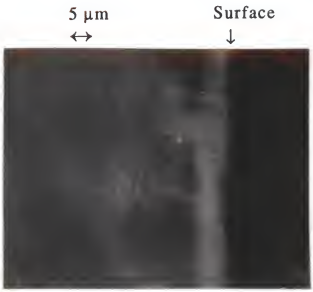

(a) Near Field

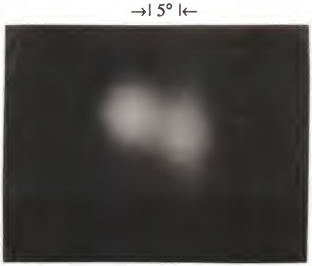

(b) Far Field

Fig. 3-15. Near and far field pictures of a bulk ZnSe laser (both at λ_p = 461 nm).

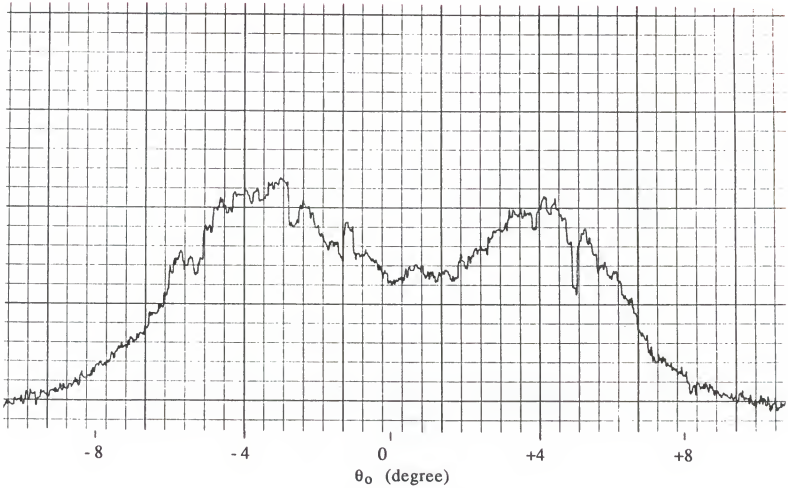

Fig. 3-16. Far field profile of a bulk ZnSe laser.

depends on how strong the gain guiding is [Bies83] and is plotted vs. λ_p for these bulk ZnSe lasers in Fig. 3-17.

In addition to showing the gain guiding effect, the near and far field profiles and their relations also provide us with data for estimating the carrier distribution and the laser mode confinement factor. Laser performance can therefore be evaluated.

3.3.3. Gain Guiding Model

Since the gain profile can not be measured directly, a certain distribution function needs to be assumed for it. Two distribution functions which give analytical solutions for near and far field profiles are in parabolic and $\cosh^{-2}$ forms. The parabolic function is not considered realistic for these lasers because it assumes infinitive loss in the unpumped region. The $\cosh^{-2}$ function is chosen partly because the near field profile calculated from it is reasonably close to what was measured and partly for the convenience of the analytical solutions it provides. The modeling, described next, starts at a fixed λ_p.

Let x be the distance from the pumped surface, g_m the maximum of optical gain g(x) and s the depth of the gain region, i.e. the x value at which g(x) reduces to 0, then g(x) can be expressed by

$$g(x) = (g_m + \alpha_i)\ \cosh^{-2}(2x/s) - \alpha_i. \tag{3.15}$$

It can be shown [Thom82] that the E component of the near field generated by such a gain profile is written as

$$E(x) = E_o\ \cosh^{-u}(2x/s), \tag{3.16}$$

where E_o is a constant and $u = u_1 + iu_2$ is a complex parameter to be determined. Illustrative g(x) and $|E(x)|^2$ curves are shown in Fig.

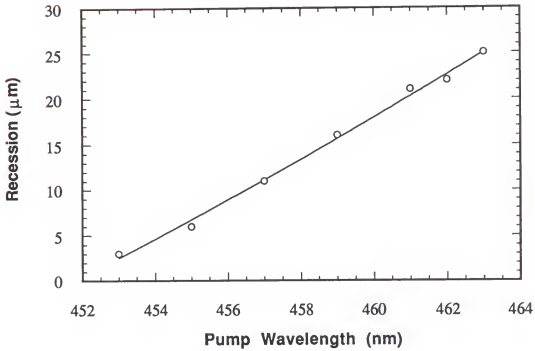

Fig. 3-17. Beam waist recession effect.

3-18. Since the nonradiative surface recombination is not considered in this model, both curves reach their maxima at $x = 0$. The drop of $|E(x)|^2$ near $x = 0$ as seen in the measured near field profile (Fig. 3-14) is believed to be due to such effect. Similar behavior is also expected for $g(x)$. As long as λ_p is not too short, the surface effect will not significantly affect $E(x)$ and $g(x)$ so that the model is valid. In Fig. 3-18, s_{eff} is the $1/e^2$ depth of $|E(x)|^2$, which can be measured from the near field profile. It can be expressed in terms of s and u_1 by letting $|E(s_{eff})|^2 = E_o^2/e^2$ in Eq. (3.16), which yields:

$$u_1 \ln[\cosh(2s_{eff}/s)] = 1. \tag{3.17}$$

The gain region depth s, which is roughly the depth within which the carriers are confined, can be calculated using the far field data as follows.

Since $u = u_1 + iu_2$ is complex, the phase front of $E(x)$ is curved. Furthermore, if u_2 is greater than u_1, the far field pattern splits into two lobes. The angular spacing θ_o between the two lobe peaks is related to u_2 by [Thom82]:

$$\sin\left(\frac{\theta_o}{2}\right) = \frac{2u_2}{ks}, \tag{3.18}$$

where $k = 2\pi/\lambda_o$. The parameter u_2 is further related to the laser cavity properties by:

$$u_2 = (2u_1 + 1)\ (b/2) - [(b^2 + 1)\ (2u_1 + 1)^2 - 1]^{1/2}, \tag{3.19}$$

where

$$u_1 = \frac{\Delta_z + \Delta_m}{2\,(\Delta_m - \Delta_z)}, \tag{3.20}$$

and

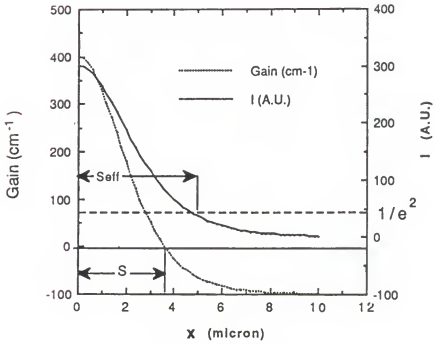

$I = |E|^2$

Fig. 3-18. Gain and optical field distribution (theoretical).

$$b = \frac{4(\Delta_m + \Delta_f)^2 - (sk)^4 (\Delta_m - \Delta_z)^4}{4 (\Delta_m + \Delta_f) (sk)^2}. \tag{3.21}$$

In Eq. (3.20) and Eq. (3.21), $\Delta_m = ng_m/k$, $\Delta_z = ng_{th}/k$ and $\Delta_f = n\alpha/k$, where n is the refractive index of ZnSe and g_{th} is the threshold gain coefficient. It can be shown that when $|b| >> 1$ and $sk >> 1$, Eq. (3.19) and Eq. (3.21) become:

$$u_2 = \frac{- kng_{th}s^2[(\Delta_f/\Delta_z) - 1]}{8u_1} \tag{3.22}$$

and

$$b = \frac{- (sk)^2 (\Delta_m - \Delta_z)^2}{4 (\Delta_m + \Delta_f)}. \tag{3.23}$$

From Eq. (3.17), (3.18) and (3.22),

$$g_{th}ns[(\Delta_f/\Delta_z) + 1] \ln[\cosh(s_{eff}/s)] = 4\sin\theta_o. \tag{3.24}$$

Therefore, s can be obtained for from Eq. (3.24) numerically. In the equation, g_{th} can be estimated from the optical gain and the I_{th} measurement, as described in Sec. 3.1 and Sec. 3.3.1. Other parameters α, s_{eff} and θ_o have all been found experimentally as functions of λ_p in the wavelength range of 455 nm to 462 nm. In Fig. 3-19, s_{eff} vs. λ_p and θo vs. λ_p are shown. Resulting s vs. λ_p relation is obtained and is illustrated along with s_{eff} vs. λ_p in Fig. 3-20. It is noticed that s decreases much faster with decreasing λ_p than s_{eff}, which implies that the portion of the laser mode located in the gain region reduces as λ_p decreases, i.e. the mode confinement factor Γ decreases with λ_p.

Mathematically, Γ can be written as [Bote84]:

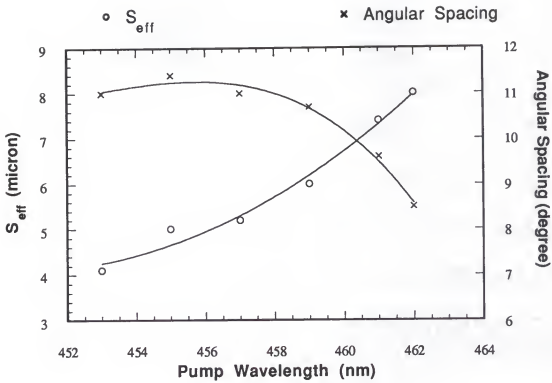

Fig. 3-19. Near field width and angular spacing of far field peaks vs. λ_p (experimental data).

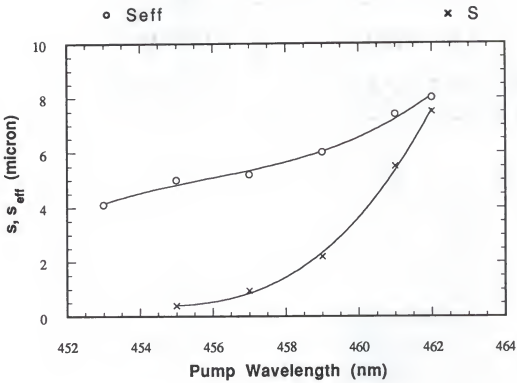

Fig. 3-20. Theoretical s (width of gain region) and s_{eff} (width of near field) vs. λ_p.

$$\Gamma = \frac{\int_0^s |E(x)|^2 dx}{\int_0^\infty |E(x)|^2 dx}. \tag{3.25}$$

The λ_p dependence of Γ is calculated using Eq. (3.16), (3.25) and the s vs. λ_p relation. It is plotted and compared with the experimental η_d vs. λ_p relation (normalized) in Fig. 3-21. It can be seen that they have the same trend but also discrepancies. This indicates that Γ can be responsible for the strong dependence of η_d on λ_p. Meanwhile, it needs to be pointed out that the assumptions made in this treatment, e.g. the $\cosh^{-2}$ gain distribution and the ignorance of surface recombination, are not sufficiently accurate. The drop in η_d on the right hand sides of Fig. 3-12 and Fig. 3-21 are attributed to the reduced laser photon generation due to smaller pump photon absorption, which is less related to Γ.

3.3.4. Comparison with Bulk GaAs Lasers

The behavior of η_d vs. λ_p of photopumped bulk ZnSe lasers may raise questions about the suitability of ZnSe as a laser medium because its η_d is generally low and is so sensitive to λ_p. In an attempt to clarify this issue, GaAs, the most commonly used laser material, was photopumped under the same conditions. An undoped (100) oriented bulk GaAs wafer was shaped into resonators similar to the ZnSe resonators shown in Fig. 2-2. The pump wavelength λ_p was tuned from 810 nm to 870 nm. Resulting spectra at various pump intensities and the η_d and I_{th} vs. λ_p relations are respectively presented in Fig. 3-22 and Fig. 3-23. It can be seen that the behavior

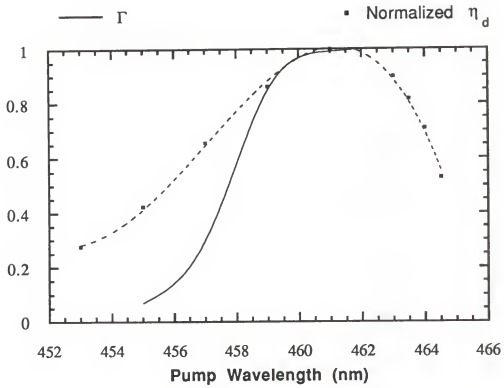

Fig. 3-21. Γ (mode confinement factor, theoretical) and experimental η_d vs. λ_p.

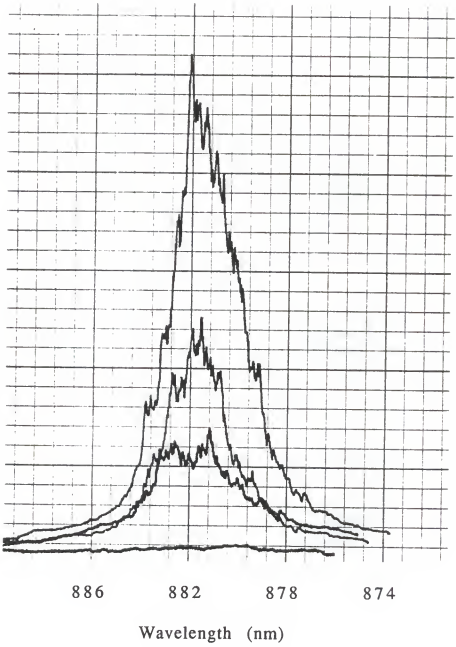

Fig. 3-22. Spectrum of a photopumped bulk GaAs laser.

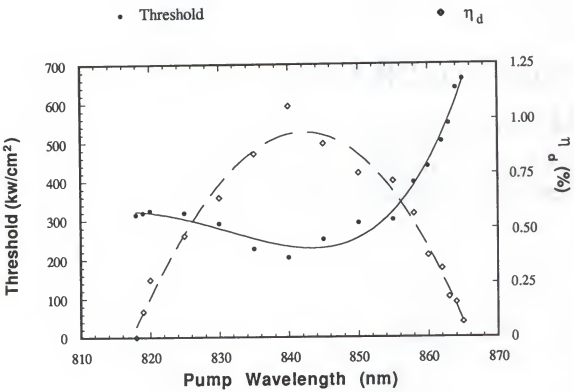

Fig. 3-23. η_d and I_{th} vs. λ_p for bulk GaAs.

of a photopumped bulk GaAs laser is very similar to that of ZnSe. The shapes of their spectra resemble each other. The magnitude of their η_d's and I_{th}'s are comparable. Especially, the λ_p dependences of η_d for the two materials are almost the same. This is better seen when η_d is normalized and λ_p is converted to the offset of pump photon energy from its optimum value (at which the maximum η_d is reached). Figure 3-24 illustrates this comparison. The close match between the two curves indicates that ZnSe can be as good as GaAs for making a laser medium. Once an appropriate confinement and current injection structure is developed, it is expected that a ZnSe based diode laser can be fabricated.

3.4. Epitaxial ZnSe Lasers

Since the goal of the photopump experiment is to develop diode lasers which are operated by current injection, as pointed out in chapter 1, carrier and optical confinement structures need to be built for a diode laser. To find the feasibility of doing this with ZnSe, photopumped epitaxial ZnSe lasers were fabricated as described in Sec. 2.1.1. It is relatively easy to grow a single layer thin film ZnSe on GaAs substrates because of their close lattice match. However, the energy band alignment and the refractive index step between the two material are not favorable for carrier and optical confinement [Kroe84, McCa90]. It is therefore questionable that if such a laser can work properly at room temperature. To find the answer, these epitaxial ZnSe lasers were photopumped at various λ_p by tuning the pump laser output from 440 nm to 460 nm. The spectrum, the P_o vs. P_p curve and the near and far field patterns (all recorded at λ_p = 450

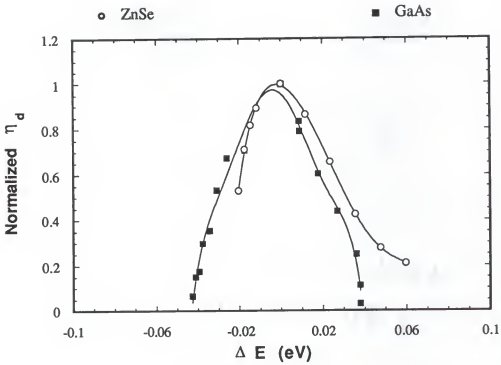

Fig. 3-24. Comparison of η_d vs. normalized ΔE between ZnSe and GaAs.

nm), as shown in Fig. 3-25 through Fig. 3-27, clearly indicate lasing. For the same reason as given in Sec. 3.3.2, the near field is believed to consist of a string of emitting elements of about 1 $\mu m \times 2\ \mu m$ in size. The result also suggests that the loss in such a structure is not likely to be as large as it might be expected. To find the reason, the λ_p dependence of the laser performance was first studied.

3.4.1. Pump Wavelength Dependence of the Laser Performance

Results on η_d vs. λ_p and I_{th} vs. λ_p for such an epitaxial ZnSe laser is given in Fig. 3-28. Both η_d and I_{th} are calculated from the P_o vs. P_p curve like the one in Fig. 3-26 at various λ_p's. They are both defined in the same manner as in Sec. 3.3. Their λ_p dependence is similar to that for the bulk ZnSe lasers to certain extent and is believed to be due to similar mechanisms (see Sec. 3.3). The waveguide loss is still expected to dominate α_i due to the lack of total internal reflection at the ZnSe/GaAs interface and the absorption in the GaAs substrate. Therefore, α_i is still a weak function of λ_p in the wavelength range shown in Fig. 3-28 and η_d vs. λ_p is mainly determined by η_i vs. λ_p. Since the laser mode in the epitaxial ZnSe laser is much better defined than in a bulk laser, the physical meaning of η_i can by seen more clearly.

Let R_p, R_G and R_{th} be the pump photon input rate, the laser photon generation rate and the threshold pump photon rate, respectively. Then $R_p = P_p/(h\nu_p) = P_p\lambda_p/(hc)$, where ν_p is the pump light frequency. Similarly, $R_{th} = P_{th}\lambda_p/(hc)$ and $R_G = P_o\lambda_o/(hc)$. Therefore, it follows from Eq. (3.13) that

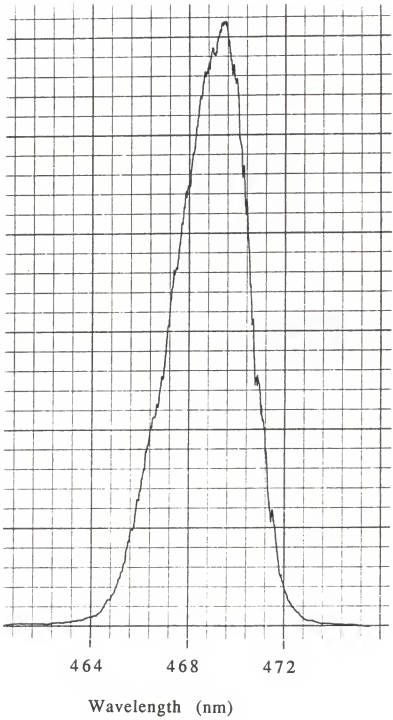

Fig. 3-25. Lasing spectra of epitaxial ZnSe

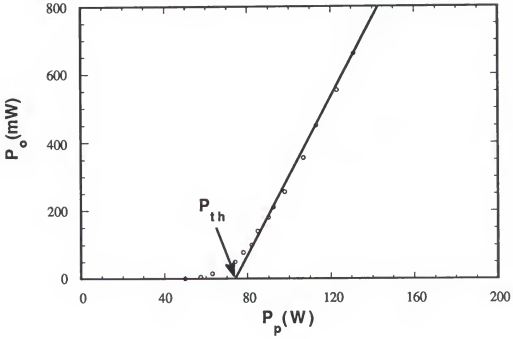

Fig. 3-26. P_o vs. P_p curve for an epitaxial ZnSe laser.

(a) Near Field

(b) Far Field

Fig. 3-27. Near and far field pictures of an epitaxial ZnSe laser.

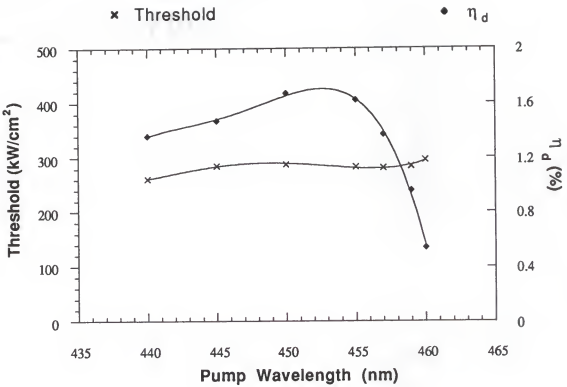

Fig. 3-28. η_d and I_{th} vs. λ_p for an epitaxial ZnSe laser.

$$\eta_i = \frac{R_G}{R_p - R_{th}}, \tag{3.26}$$

hence,

$$\eta_i R_p = \eta_i R_{th} + R_G. \tag{3.27}$$

Suppose R_{sp} and R_{nr} are the spontaneous emission photon rate and the nonradiative recombination photon rate in the laser mode volume, respectively. Let η_n be the fraction of pump photons being converted to carriers, which recombine in the laser mode volume. Since laser photons are always generated in the laser mode volume, in steady state, photon conservation in the volume requires that

$$\eta_n R_p = R_{sp} + R_{nr} + R_G. \tag{3.28}$$

At the threshold, no laser photons are generated, therefore $R_G = 0$. It follows from Eq. (3.28) that

$$\eta_n R_p = \eta_n R_{th} = R_{sp} + R_{nr}. \tag{3.29}$$

Since the carrier density in the laser mode volume is clamped at its threshold level when R_p goes beyond R_{th} [Biar64], the second equation of Eq. (3.29) is also valid for above threshold situation provided that η_n remains constant. Eq. (3.28) can therefore be written as

$$\eta_n R_p = \eta_n R_{th} + R_G. \tag{3.30}$$

By comparing Eq. (3.27) and Eq. (3.30), we have

$$\eta_n = \eta_i. \tag{3.31}$$

When $R_p >> R_{th}$, it can further be seen from Eq. (3.27) and Eq. (3.30) that $\eta_n \approx \eta_i$ is still valid even if η_n changes with R_p. Therefore, η_i is actually the fraction of pump photons being converted into carriers, which recombine in the laser mode volume. As λ_p changes, η_i can thus be reduced in two manners: (a) at certain λ_p's, pump photons

are not absorbed in or near the laser mode volume due to inappropriate α and (b) carriers recombine nonradiatively outside the lasing mode (e.g. at the surface) before they diffuse into the mode volume to contribute to lasing.

Based on this theory, the η_d vs. λ_p curve in Fig. 3-28 can be qualitatively interpreted as follows. Near the right end of each curve in Fig. 3-28, η_d is low, because much reduced α causes pump photons and carriers to penetrate deep enough that they are lost outside the laser mode volume. As λ_p decreases, η_d grows because increasing α prevents excess pump photon penetration so that more carriers are generated inside or nearby the mode volume. These carriers thus have greater probability to recombine radiatively in the laser mode and contribute to lasing. As λ_p decreases furthermore, very large α results in little penetration of pump photons, which causes smaller amount of carriers to be generated in the laser mode volume and most of them generated very close to the surface. The carriers near the surface tend to recombine nonradiatively at the surface before having a chance to diffuse into the mode volume and to contribute to lasing. η_d is thus lowered once again.

Since the laser mode in the epitaxial ZnSe laser is well defined and is independent of λ_p, the η_d vs. λ_p and I_{th} vs. λ_p relations can be modeled better than for a bulk laser. By using waveguide theory and the continuity equation, both the laser mode profile and the carrier distribution can be calculated more accurately. With the α vs. λ_p relation known, they can be converted to the relative changes of η_d and I_{th} with λ_p and compared with experimental data. Such semi-quatitative treatment is presented next.

3.4.2. Continuity Equation Model

Carrier distribution in a semiconductor material is governed by the continuity equation, for the one dimensional situation [Hwan69],

$$D\frac{d^2n(x)}{dx^2} - \frac{n(x)}{\tau} + G\exp(-\alpha x) = 0. \tag{3.32}$$

In the above equation, x is the distance from the surface, n(x) is the carrier density at x, τ is carrier lifetime, G is carrier generation rate at the surface and D and α are the diffusivity of the carriers and the optical absorption coefficient of the material. For a photopumped laser, the carriers are generated at the surface (x = 0) by pump light, therefore:

$$G = \left(\frac{1}{h\nu}\right)\left(\frac{dI_p(0)}{dx}\right), \tag{3.33}$$

where $I_p(0)$ is the pump light intensity at the surface. The boundary conditions for Eq. (3.32) are determined by the behavior of carriers at the surface (x = 0) and the ZnSe/GaAs interface (x = t = 1 μm). Non-radiative surface recombination makes the surface behave as a carrier sink. If v_s is the surface recombination velocity, such a process can be written as:

$$\frac{dn(0)}{dx} = \frac{v_s}{D}\,n(0). \tag{3.34}$$

It is not yet clear what the most appropriate expression is for the behavior of carriers at the x = t interface. Conservatively speaking, however, the carrier population must diminish after being created at

small x's and traveling deep enough into the material. Therefore, the other boundary condition is written as

$$n(\infty) = 0. \tag{3.35}$$

Eq. (3.32) can be solved analytically using Eq. (3.34) and Eq. (3.35). Let $L = (D\tau)^{1/2}$ be the diffusion length of carriers, the solution to Eq. (3.32) is obtained as

$$n(x) = \frac{\alpha I_p(0) L^2}{h\nu D(1 - \alpha^2 L^2)} \left[\exp(-\alpha x) - \frac{\alpha + (v_s/D)}{(1/L) + (v_s/D)} \exp\left(-\frac{x}{L}\right)\right], \tag{3.36}$$

which is plotted for large and small α, corresponding to short and long λ_p, in Fig. 3-29. It can be seen that at short λ_p, the carriers are found closer to the surface and their concentration is higher. At longer λ_p's, the carriers spread more into the material and their peak concentration is lower.

The laser mode profile can be obtained by solving the electromagnetic field equations (for TE_0 mode) [Hall73] for this waveguide structure (Fig. 3-30):

$$\begin{aligned} E_y(x) &= A \exp(ih_3 x) && (x > t) \\ E_y(x) &= B \cos(h_2 x) + C \sin(h_2 x) && (0 < x < t) \\ E_y(x) &= D \exp(-ih_1 x) && (x < 0) \end{aligned} \tag{3.37}$$

where $h_1 = ik_2[1 - (\varepsilon_1/\varepsilon_a)]^{1/2}$, $h_2 = (\pi/t^2)[t - (f_2/k_2) - i(f_3/k_3)]$, $h_3 = k_2[(\tilde{\varepsilon}_c/\varepsilon_a) - 1]^{1/2}$, $f_2 = [1 - (\varepsilon_1/\varepsilon_a)]^{-1/2}$, $f_3 = [(\tilde{\varepsilon}_c/\varepsilon_a) - 1]^{-1/2}$, $k_2 = (2\pi/\lambda)(\varepsilon_a/\varepsilon_0)$, $k_3 = (2\pi/\lambda)(\tilde{\varepsilon}_c/\varepsilon_0)$, and A, B, C and D are constants. At the output wavelength of these lasers (λ = 469 nm), the dielectric constants are known to be $\varepsilon_1 = \varepsilon_0$, $\varepsilon_a = 7.87\varepsilon_0$, and $\tilde{\varepsilon}_c = (20.50 + i5.435)\,\varepsilon_0$ [Wang81]. Therefore, $E_y(x)$ in the ZnSe layer ($0 < x < t$) can be solved for from Eq. (3.37), which yields

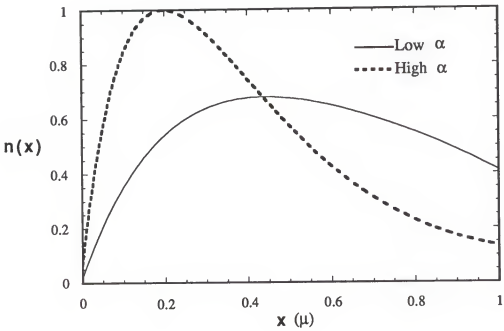

Fig. 3-29. Theoretical n(x) at various α (i.e. various λ_p).

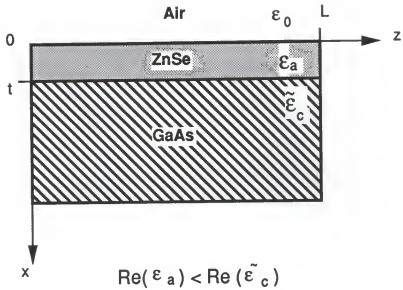

Fig. 3-30. Leaky guide structure.

$$E_y(x) = C[\sin(1.55x) + 6.29\times10^{-3}\cos(1.55x) + 3.05\times10^{-2}\cos^2(1.55x)], \tag{3.38}$$

where C is a constant. The laser light intensity distribution $I_o(x)$ is thus obtained as

$$I_o(x) = E_y^*(x)\, E_y(x) = C^2[\sin^2(1.55x) + 6.29\times10^{-3}\sin(3.09x)]. \tag{3.39}$$

Both n(x) and $I_o(x)$ are plotted in Fig. 3-31 for various α's. The $I_o(x)$ profile is usually called the laser mode profile. It is interesting to notice that the laser mode is almost completely confined in the ZnSe active layer although a negative refractive index step exists between the active and the cladding layer. A physical interpretation on this is to be given in Sec. 3.4.5. It can also be shown that the peak intensity of the laser mode is always found near the middle of the active layer (x = 0.5t) for this type of structure regardless the value of t.

It has been established in Sec. 3.3 that η_d vs. λ_p relation mainly depends on the η_i vs. λ_p relation. It was also shown that η_i is actually the fraction of pump photons converted to carriers, ending up in the laser mode volume. Since the mode volume for these epitaxial ZnSe lasers is the ZnSe active layer ($0 < x < t$ in Fig. 3-30), η_d is thus proportional to the total amount of carriers in the active layer in steady state. Quantitatively, for a fixed pump intensity $I_p(0)$,

$$\eta_d = \kappa \int_0^t n(x)\, dx, \tag{3.40}$$

where κ is a constant. Substituting Eq. (3.36) into Eq. (3.40), η_d at various α, i.e. various λ_p, can be calculated. The result for λ_p = 440 nm to 465 nm is shown and compared with experimental η_d in Fig. 3-32. Note that both theoretical and experimental η_d's have been

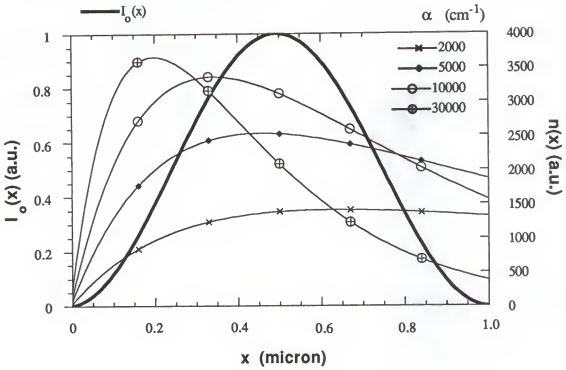

Fig. 3-31. Theoretical $I_0(x)$ and n(x) at various α.

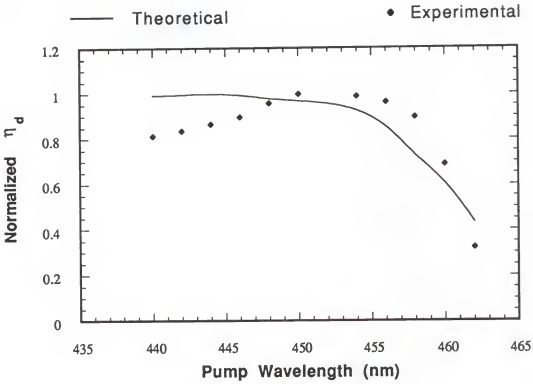

Fig. 3-32. Comparison between theoretical and experimental $\eta_d(\lambda_p)$.

normalized for making a direct comparison. In the calculation, L = 0.5 μm [Gaut82] and $v_s/D = 10^6$ cm^{-1} [Nag80] were assumed. They were not measured here for the laser material used in this work. The discrepancy at the short λ_p side is believed to mainly come from the inaccurate estimate of these values.

The threshold pump intensity I_{th} needs to be calculated from the threshold mode gain G_{th}. For a DH laser, G_{th} is conventionally defined as [Case78]

$$G_{th} = \Gamma\ g_{th}, \tag{3.41}$$

where Γ is the same as defined in Eq. (3.25). g_{th} is the threshold gain in the active layer and is assumed to be uniform, i.e. $g_{th} \neq g_{th}(x)$. For the ZnSe epitaxial lasers being studied here, g_{th} varies with x because the carriers are not well confined. G_{th} thus has to be derived from the original threshold condition.

Suppose the laser light propagates in z direction between z = 0 to z = L, as shown in Fig. 3-30. The light intensity I_o can then be written as

$$I_o(z) = I_x\ i(z), \tag{3.42}$$

where

$$I_x = \int_0^{+\infty} i(x)\ dx. \tag{3.43}$$

In writing the above two equations, it has been assumed that the x dependence of I_o does not change with z and the variation of I_o in the third dimension has been ignored, i.e. $I_o(x,z) = i(x)i(z)$. Like $I_o(x)$ in Eq. (3.39), i(x) describes the laser mode profile, . Let g be the optical gain and assume that g does not depend on z, i.e. g = g(x). According to the definition of gain, I_o satisfies

$$\frac{dI_o(x,z)}{dz} = [g(x) - \alpha_i]\, I_o(x,z), \tag{3.44}$$

where α_i is the optical loss defined earlier. By integrating both sides of the above equation with respect to x and using Eq. (3.42) and (3.43), we have

$$\frac{d}{dz}[I_o(z)] = I_o(z)\,[\frac{1}{I_x}\int_0^{+\infty} g(x)i(x)dx - \alpha_i\,]. \tag{3.45}$$

Define mode gain G as

$$G \equiv \frac{1}{I_x}\int_0^{+\infty} g(x)i(x)dx. \tag{3.46}$$

Eq. (3.45) then becomes

$$\frac{d}{dz}[I_o(z)] = I_o(z)\,[G - \alpha_i]. \tag{3.47}$$

Eq.(3.47) is of the same form as the standard differential equation for finding the threshold gain of a laser [Thom82]. By solving Eq. (3.47) and using the threshold condition, the threshold gain G_{th} can be obtained as

$$G_{th} = \alpha_i + [\ln(1/R_o)]/L. \tag{3.48}$$

Using Eq. (3.25), it can also be easily shown that G_{th} reduces to that given in Eq. (3.41) if g_{th} is constant in the active layer and zero elsewhere. It is known from Eq. (3.48) that G_{th} is essentially independent of λ_p in the range shown in Fig. 3-28 because it has been established earlier that all the parameters on the right hand side do not depend strongly on λ_p. Therefore, the λ_p dependence of I_{th} must come from the λ_p dependence of i(x) and g(x), according to Eq. (3.46). Since [Biar64]

$$g(x) = \chi\ [n(x)\ -n_{tr}], \tag{3.49}$$

where n_{tr} is the n(x) value when the material is transparent and χ is a constant, at threshold, Eq. (3.46) becomes

$$G_{th} = \frac{\chi}{I_x}\int_0^{+\infty} n_{th}(x)i(x)dx\ -\ \frac{\chi n_{tr}}{I_x}\int_0^{+\infty} i(x)dx. \tag{3.50}$$

According to Eq. (3.36), $n(x) = \xi I_p(0)n_o(x)$, where ξ is a constant and $n_o(x)$ is the n(x) at certain fixed $I_p(0)$, which can be considered as the normalized carrier distribution function. At threshold, n(x) thus becomes

$$n_{th}(x) = \xi I_{th} n_o(x). \tag{3.51}$$

Substitute Eq. (3.43) and (3.51) into Eq. (3.50), I_{th} can be expressed as

$$I_{th} = \frac{I_x}{\chi\xi} \times \frac{G_{th} + \chi n_{tr}}{\int_0^{+\infty} n_o(x)i(x)dx}.$$

Since I_x, χ, ξ, G_{th} and n_{tr} are all constants when λ_p changes, I_{th} can be written as

$$I_{th} = \frac{K}{\int_0^{+\infty} n_o(x)i(x)dx}, \tag{3.52}$$

where K is another constant. Eq. (3.52) indicates that I_{th} not only depend on whether the carriers are found within the mode volume, but also on how they distribute and overlap with the mode profile. Once again, as $n_o(x)$ changes with λ_p, I_{th} vs. λ_p can be obtained from Eq. (3.52). The relation is illustrated and compared with the experimental data in Fig. 3-33. The values were also normalized to facilitate comparison. There is a growing discrepancy between the

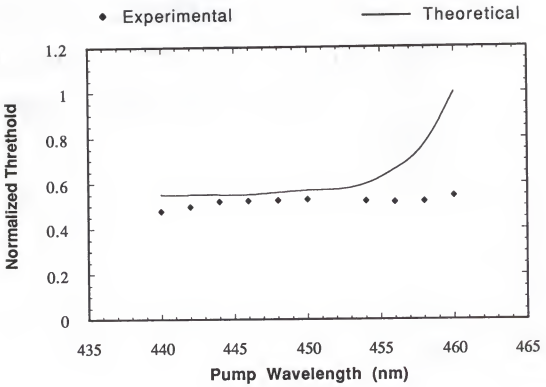

Fig. 3-33. Comparison between theoretical and experimental $I_{th}(\lambda_p)$.

experiment and the theory on the long λ_p side. This can be partly attributed to the boundary condition Eq. (3.35), which may not be appropriate for this type of structure.

3.4.3. Epilayer Thickness Dependence of the Laser Performance

The results on η_d vs. λ_p and I_{th} vs. λ_p relations were obtained at a fixed epilayer thickness, t = 1μm. When t changes, the boundary conditions for Eq. (3.32) and Eq. (3.37) will also change, resulting in different solutions for n(x) and $I_o(x)$. Consequently, η_d vs. λ_p and I_{th} vs. λ_p relations are expected to vary. Qualitatively speaking, since the carrier and optical confinement ability of the structure changes with t, the λ_p dependence of both η_d and I_{th} changes. Their optimum values and corresponding λ_p's, as well as the sensitivity of their λ_p dependence will all vary. By studying such variations, we can find the optimum t for this type of structure and to verify the validity of the model used in Sec. 3.3 as well.

Experimental results on η_d vs. λ_p and I_{th} vs. λ_p relations for t = 0.5 μm, 1.0 μm, 1.5 μm, 3.5 μm and ∞ (bulk ZnSe) are illustrated in Fig. 3-34 and Fig. 3-35. Although the data come from lasers made from different type of ZnSe, i.e. MBE, MOCVD and melt-grown, it turns out that their performance depend much more on t than on the type of the material. In Fig. 3-34, it is noticed that as t increases, the maximum η_d grows and the λ_p at which the η_d reaches its maximum gets longer. Meanwhile, the λ_p dependence of η_d becomes stronger, i.e. the peak of the η_d vs. λ_p curve becomes sharper. This is due primarily to the fact that as t increases, the laser mode spreads more from the surface and the nonradiative surface recombination

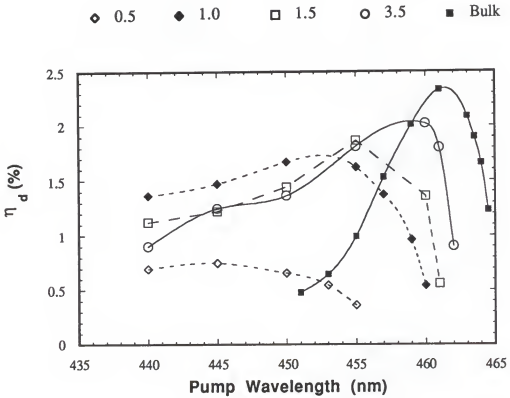

Fig. 3-34. $\eta_d(\lambda_p)$ for various epilayer thicknesses (in μm, as shown in legend).

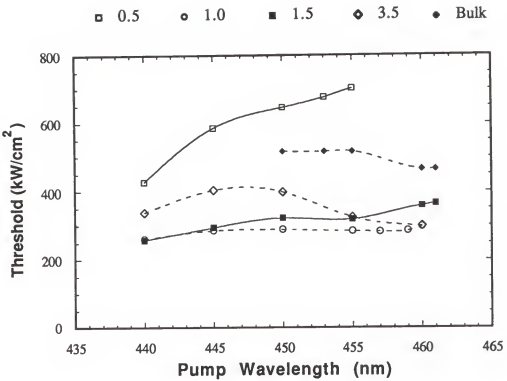

Fig. 3-35. $I_{th}(\lambda_p)$ for various epilayer thicknesses (in μm, as shown in legend)

becomes less dominant. Therefore, the maximum total amount of carriers found in the active layer increases with increasing t, resulting in larger maximum η_d according to Eq. (3.40). Since the optical absorption coefficient α decreases with λ_p (see Sec. 3.2), this maximum amount of carriers created by pump light is built up at longer λ_p for a larger t. Understandably, near maximum amount of carriers should only be reached in very small range of λ_p for any t's. This is actually the case only for relatively large t's. When t is small, because of the significant surface recombination loss, such maximum can never be approached. Consequently, the η_d is clamped at a lower value for a relatively larger λ_p range and the corresponding curve is less sharp. More physical interpretation of these curves is to be given in next section when the epitaxial and bulk ZnSe lasers are compared.

The threshold pump intensity I_{th} is much less sensitive to λ_p than the η_d for lasers of all t's (see Fig. 3-35). With certain exceptions, the λ_p at which the maximum η_d is reached is roughly the λ_p for the minimum I_{th} is obtained for a given t. But the t dependence of the minimum I_{th} is not monotonic. The optimum t in terms of I_{th} is about 1 μm. The bulk laser ($t \sim \infty$), although has the best maximum η_d, turns out to have the second highest overall I_{th}. The reason is believed to be that the carrier profile in a bulk laser can not match the laser mode as closely as in an epitaxial laser under photopump. The final choice of t should be based on the consideration of both η_d and I_{th}.

3.4.4. Comparison with GaAs Lasers and Bulk ZnSe Lasers

To illustrate the difference the epitaxial structure makes to the performance of a ZnSe laser, a typical η_d vs. λ_p curve of an epitaxial ZnSe laser is compared directly to that of a bulk ZnSe laser in Fig. 3-36. It is noticed that η_d is not high for both epitaxial and bulk lasers because of the absence of a DH-like structure and the surface recombination. Since the bulk laser has a deeper mode peak location and does not suffer the additional non-radiative recombination at the ZnSe/GaAs interface, it has a larger maximum η_d than the epitaxial ZnSe laser and its maximum η_d is found at longer λ_p. Because the mode in the bulk laser spreads more than the mode in the epitaxial laser, η_d of the bulk laser drops faster on the short wavelength side of the η_d vs. λ_p curve. The relative insensitive λ_p dependence of η_d for epitaxial lasers can be seen more clearly when the two curves are converted into normalized η_d vs. energy offset ΔE relations, as shown in Fig. 3-37, where ΔE is the offset of pump photon energy from its optimum value at which the maximum η_d is reached. It is believed that such insensitivity is due primarily to the well defined TE_0-like λ_p independent lasing mode existing in such lasers, which is discussed next.

3.4.5. Leaky Waveguide Model

As mentioned earlier, the major optical loss of this structure, waveguide loss α_{wg}, is easily expected to be large because of the negative refractive index step at the ZnSe/GaAs interface and the high absorption coefficient of the GaAs to laser photons. However, as we will show below, α_{wg} can be small at blue wavelengths for this

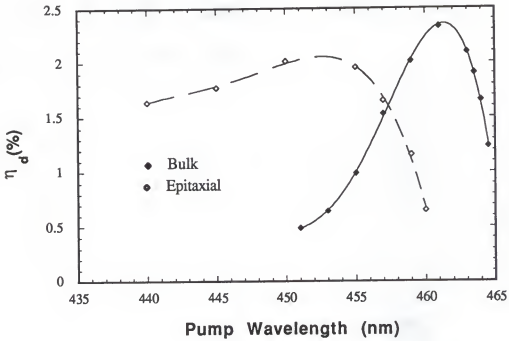

Fig. 3-36. Comparison of $\eta_d(\lambda_p)$ between bulk and epitaxial ZnSe lasers.

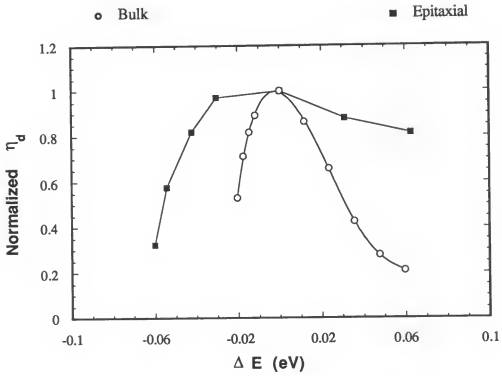

Fig. 3-37. Comparison of normalized η_d vs. ΔE between bulk and epitaxial ZnSe.

structure and consequently, relatively small α_i and high η_d can be maintained in blue (see Eq. (3.13) and (3.14)).

By leaky waveguide theory [Hall73], α_{wg} can be calculated for a known laser mode. Polarization and far field pattern measurements showed that lasing appears to occur on the TE_0 mode of the antiguide. Since the strong mode discrimination of an anti-guide suppresses higher order modes significantly, it is believed that the existing laser mode is dominated by TE_0. Therefore, the diffraction loss α_{wg} of this structure can be written as

$$\alpha_{wg} \cong \left(\frac{\lambda_o^2}{2t^3}\right) \mathrm{Re}\left\{\frac{\varepsilon_0}{[\varepsilon_a(\tilde{\varepsilon}_c - \varepsilon_a)]^{1/2}}\right\} \tag{3.53}$$

where ε_0 and ε_a are respectively the dielectric constants of the air and ZnSe, which are essentially real and do not depend strongly on wavelength in visible and infrared range and $\tilde{\varepsilon}_c$ is the complex dielectric constant of GaAs. The above expression is an approximation for TE_0 mode in near plane-wave situation [Hall73], which is considered to be our case because the structure is far from cut-off for the TE_0 mode.

It is noticed in Eq. (3.53) that the λ_o^2 dependence makes α_{wg} much smaller at blue wavelengths than in the infrared. In addition, as λ_o decreases from infrared to blue, the change of $\mathrm{Re}(\tilde{\varepsilon}_c)$ with wavelength (about $9\varepsilon_0$) [Wang81] further lowers α_{wg} by about a factor of 2. The structure is also a strong antiguide at $\lambda_o \sim 470$ nm because $\mathrm{Re}(\tilde{\varepsilon}_c) - \mathrm{Re}(\varepsilon_a)$ is large [Wang81]. This large difference (about $12\varepsilon_0$) significantly reduces the transmission loss at the interface. The $\mathrm{Im}(\tilde{\varepsilon}_c)$, which is not negligible at 470 nm, makes the substrate

somewhat metallic, further lowering α_{wg} [Luo90]. The overall wavelength dependence of α_{wg} is illustrated in Fig. 3-38.

It is interesting to note that $\alpha_{wg} \sim 80\ cm^{-1}$ at blue wavelengths is only about a factor of 4 higher than the internal loss of a conventional DH AlGaAs laser [Kres77]. The low loss of this structure is also evidenced by its I_{th} data (~350kW/cm^2), which is comparable to the I_{th} (500kW/cm^2) of a photopumped ZnCdSe/ZnSe multiple quantum well laser of the same cavity length with positive index step confinement [Jeon90]. Since the losses are reasonably low and the beam quality is good, due to the TE_0-like mode, this type of novel antiguide structure is believed to have the potential to be developed into devices like blue superluminescent edge light emitting diodes (ELEDs) and array ELEDs for optical storage applications. Short wavelength, high output power with good beam quality would be the main advantages of such devices [Li90].

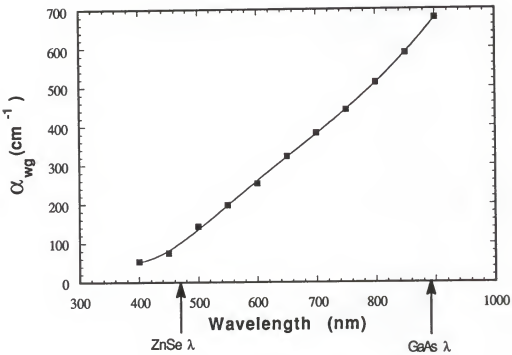

Fig. 3-38. $\alpha_{wg}(\lambda_o)$ for the ZnSe on GaAs leaky guide.

CHAPTER 4
SUMMARY AND PROPOSALS

In this work, the prospect of fabricating ZnSe based diode lasers has been surveyed in many aspects. The results turn out to be quite promising. Most of them indicate that this type of blue laser can be realized in the near future after further progress is made in p-type doping and carrier confinement. The main issues addressed in this work include the following:

For the material, optical gain and absorption properties of ZnSe were measured. It was found that the gain can be sufficiently large to realize lasing and the absorption saturation can significantly affect the carrier and laser mode profiles and their confinement.

Laser mode confinement abilities were evaluated. The mode profiles were measured directly from near field patterns. For the bulk laser, it was shown that the mode can be confined by gain guiding, which enables the laser to oscillate. For the antiguide epitaxial laser, the mode profile was calculated using leaky waveguide theory and was shown to be well confined in the ZnSe epilayer, which demonstrates the feasibility of fabricating novel antiguide blue emitters.

Carrier confinement abilities were also evaluated. For the bulk laser, the carrier distribution was estimated using a unique approach, beam characteristic analysis. The result is that both the carrier

distribution and the η_d depend strongly on λ_p, which indicates that the carrier confinement is critical for the performance of this type of lasers. The carrier distribution for the epitaxial lasers was calculated using a continuity equation model. It also directly affects η_d. Material properties of ZnSe make it very difficult to confine carriers by using a conventional DH structure. A novel confinement configuration is to be proposed in this chapter.

Electrical properties of this type of devices were studied preliminarily by analyzing the I-V characteristics and the light output spectrum of an ELED fabricated from structures grown at this university. This result is to be presented next.

Throughout this work, tunable photopump has been used extensively. Most results come from the pump wavelength dependence of the variables. It proves that tunable photopump is a efficient and convenient tool for developing new diode laser materials and structures.

Although a ZnSe based diode laser has not been realized at this point of the research, some proposals which are deemed reasonable and promising based on the results of this work are presented next for the benefit of the people who are working in this area and who believe the goal can be accomplished.

It should be maintained that to fabricate current injection devices similar to standard, high efficiency diode lasers, cladding materials with higher energy bandgaps and lower refractive indices than ZnSe are needed. A straddled energy band alignment [Kroe84] is usually desired to confine both electrons and holes in the ZnSe active layer. The materials must also be able to be appropriately

doped in order to form a p-n junction. Such cladding materials for ZnSe have not yet been demonstrated. However, if a staggered energy band alignment [Kroe84] is created by using appropriate low bandgap materials and proper doping and bias, at least one type of carrier can be efficiently injected into the active layer regardless the bandgap of cladding materials. Electrons and holes can be injected separately from each side of the active layer by using different cladding materials as illustrated in Fig. 4-1. From a carrier injection and confinement point of view, the staggered heterojunction structure is equivalent to a homojunction. However, from a photon point of view, the staggered structure is superior to a homojunction because of the waveguiding effect from the real refractive index step (which can be negative, as the antiguide shown in last chapter). Consequently, the beam quality will be better than in a homojunction device because the lasing mode is TE_0-like, as discussed earlier. Therefore, it is believed that this type of novel antiguide double heterojunction (ADH) structure has the potential to be developed into superluminescent blue light emitting diodes and diode arrays for optical storage applications.

The structure of such a proposed ADH edge light emitter is shown in Fig. 4-2. Because the goal is the get blue light output, ZnSe is a favored candidate material for the active layer. ZnSSe and CdSSe also seem to be possible. The substrate material is likely to be GaAs for the consideration of lattice match, doping and processing. The candidate materials for cladding layers may be ZnSSe, ZnTe, CdS, GaAs, etc. The selection is to be based on their energy band offsets and lattice match with the active layer and the cladding layer. There

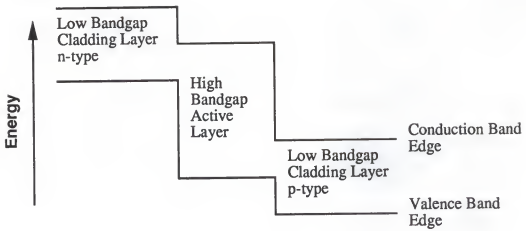

Fig. 4-1. Energy band diagram of a proposed ADH structure.

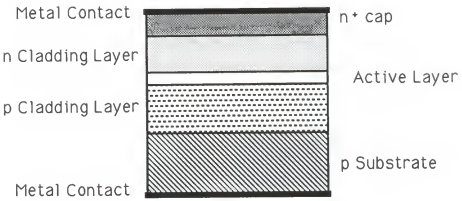

Fig. 4-2. Structure of a proposed ADH emitter.

have been many reports on these data [McCa90, Kass90] but they need to be verified for the individual samples used for fabricating the structure because those reported data were obtained under specific conditions and the doping in those samples may not be suitable for making diode lasers.

Another issue for fabricating current injection devices is the electrical contacts and some built-in potential barriers which are likely to exist at some interfaces between the layers. Thanks to the availability of a p-n junction ZnSe sample from the Materials Science and Engineering Department of the University of Florida, this problem was studied before an ADH is actually fabricated. By putting metal contacts onto their samples [Park90b], ZnSe ELED arrays were fabricated. The structure is shown in Fig. 4-3 and the current-voltage (I-V) curve is given in Fig. 4-4. It was found that the diode couldn't be "turned on" at the beginning until forward biased to about 45 V (Fig. 4-4a). This may be attributed to the large built in potential at the p-ZnSe and p-GaAs interface [Park90b]. Once a little higher voltage was applied, the turn-on voltage dropped to about 25 V and stayed at that value (Fig. 4-4b). It is not yet clear exactly what type of breakdown happened in the diode and where it happened, at the metal-semiconductor interface or between the semiconductor layers. Nevertheless, once the turn-on voltage of the diode has been lowered using such "voltage breakdown", blue light emission can be obtained from the edge of the diode. The output light spectra measured at a current of about 10 milliamperes is presented in Fig. 4-5. It is noticed that its spectral width is similar to that of the surface emitting LED made from the same structure [Park90b], which

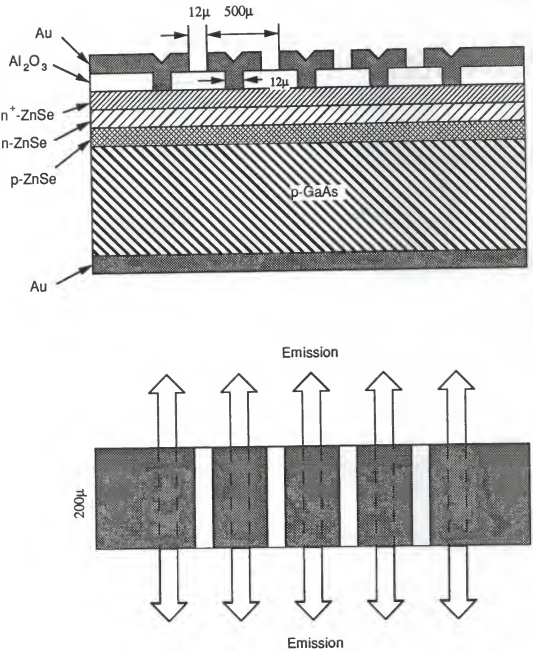

Fig. 4-3. A ZnSe LED array. (Top: side view, bottom: top view)

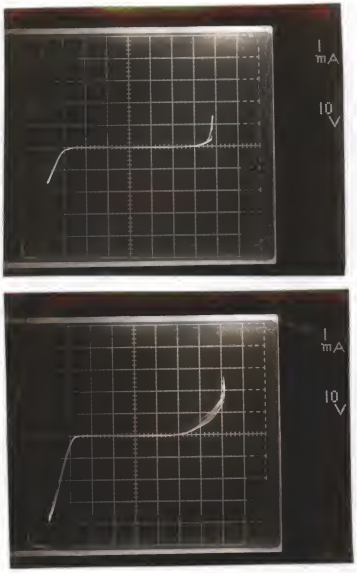

(a)

(b)

(a) Before breakdown
(b) After breakdown

Fig. 4-4. I-V characteristics of a ZnSe ELED.

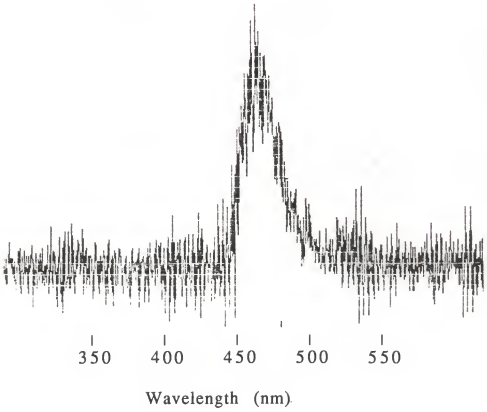

Fig. 4-5. Spectra of a forward biased ZnSe ELED.

indicates the lack of gain in the ELED. Once the allowed operation current can be raised to the equivalent excitation intensity range shown in Fig. 3-4, gain in lateral direction would be obtained and the output spectral narrowed (cf. Sec. 3.1). Output power, efficiency and beam quality would then be significantly improved. This preliminary result shows that once some technical problems have been solved, this type of ELEDs may become the first for practical uses and the array ELEDs may be used for individually addressable optical reading/writing heads.

Finally, the author would like to point out that most of the models and theory presented in this work are in their very early stage of development. There is a lot of room for improving the models, especially their accuracy, after more data on the optical properties of ZnSe material are available. It is the author's wish that these first stage results would be of value for the final achievement of room temperature operation of a ZnSe based laser diode.

REFERENCES

[Agra86] G. P. Agrawal and N. K. Dutta, *Long Wavelength Semiconductor Lasers*, Van Nostrand Reinhold, New York, 1986.

[Akim90] K. Akimoto, T. Miuajima, and U. Mori, Japanese J. Appl. Phys., vol. 29, pp. L529-L534, 1990.

[Alle 73] J. W. Allen, J. Luminescence, vol. 7, pp. 228-240, 1973.

[Ando85] H. Ando, H. Inuzuka, M. Konagai, and K. Takahashi, J, Appl. Phys., vol. 58, pp. 802-805, 1985.

[Asbe79] P. M. Asbeck, D. A. Cammack, J. J. Daniele, and V. Klebanoff, IEEE J. Quantum Electron., vol. QE-15, pp. 727-733 , 1979.

[Aven61] M. Aven, D. T. F. Marple and B. Segall, J. Appl. Phys., vol. 32, pp. 2261-2265, 1961.

[Bakk77] J. Bakker, and G. A. Acket, IEEE J. Quantum Electron., vol. QE-13, pp. 567-573, 1977.

[Biar64] H. R. Biard, W. N. Carr, and B. S. Reed, Trans. Met. Soc. AIME, vol. 230, pp. 286-290, 1964.

[Bies83] J. W. M. Biesterbos, R. P. Brouwer, A. Valster, J. A. de Poorter, and G. A. Acket, IEEE J. Quantum Electron., vol. QE-19, pp. 961-965, 1983.

[Bote84] D. Botez, RCA Review, vol. 45, pp. 23-32, 1984.

[Byls85] R. B. Bylsma and W. M. Becker, Appl. Phys., Lett., vol. 47, pp. 1039-1041, 1985.

[Camm87] D. A. Cammack, R. J. Dalby, H. J. Cornclissen, and J. Khurgin, J. Appl. Phys., vol. 62, pp. 3071-3074, 1987.

[Case78] H. C. Casey and M. B. Panish, *Heterostructure Lasers*, Academic Press, New York, 1978.

[Cata82] I. M. Catalano, A. Cingolano, M. Ferrara, and M. Lugara, Solid State Comm., vol. 43, pp. 371-374, 1982.

[Chun90] M. K. Chun and L. Goldberg, IEEE LEOS Annual Conference, Paper ELT8.2, Boston, Mass., Nov. 4-9, 1990.

[Cons91] J. A. Constance, IEEE The Institute, vol. 15, p. 3, 1991.

[Cook79] D. D. Cook, and F. R. Nash, J. Appl. Phys., vol. 46, pp. 1669-1672, 1984.

[Dixo90] G. J. Dixon, IEEE LEOS Annual Conference, Paper ELT8.1, Boston, Mass., Nov. 4-9, 1990.

[Dumk62] W. P. Dumke, Phys. Rev., vol. 127, pp. 1559-1563, 1962.

[Era70] K. Era, and D. W. Langer, J. Luminescence, vol. 1,2, pp. 514-527, 1970.

[Feit88] D. G. Feitelson, *Optical Computing*, The MIT Press, Cambridge, 1988.

[Gaut82] J. Gautron and Pl. Lemassaon, J. Crystal Growth, vol. 59, pp. 332-337, 1982.

[Glas88] A. M. Glass and K. Tai, Apll. Phys. Lett., vol.53, pp.834-836, 1988.

[Gree89] W. B. Green, *Digital Image Processing*, Van Nostrand Reinhold, New York, 1989.

[Guan90] Y. Guan, C. A. Zmudzinski, and P. S. Zory, IEEE LEOS Annual Conference, Paper SDL7.3, Boston, Mass., Nov. 4-9, 1990.

[Guns88] R. L. Gunshor and L. A. Kolodziejski, IEEE J. Quantum Electron. vol. 24, pp.1744-1757, 1988.

[Hall73] D. B. Hall and C. Yeh, J. Appl. Phys. vol. 44, pp. 2271-2274, 1973.

[Hech79] E. Hecht and A. Zajac, *Optics*, Addison Wesley, Reading, Mass., 1979.

[Hwan69] C. J. Hwang, Appl. Phys. Lett., vol. 40, pp. 3731-3739, 1969.

[Jain88] F. C. Jain, J. Crystal Growth, vol. 86, pp. 929-931, 1988.

[Jeon90] H. Jeon, J. Ding, A. V. Nurmikko, H. Luo, N. Samarth, J. K. Furdyna, W. Q. Bnner, and R. E. Nahory, Appl. Phys. Lett vol. 57, pp. 2413-2415, 1990.

[John71] W. D. Johnston, J. Appl. Phys. Lett. vol. 42, pp. 2731-2740, 1971.

[Kass90] L. Kassel, H. Abas, J. W. Garland, and P. M. Raccah, Appl. Phys. Lett. vol. 56, pp. 42-44, 1990.

[Kitt76] C. Kittek, *Introduction to Solid State Physics*, McGraw Hill, New York, 1976.

[Kres77] H. Kressel and J. K. Butler, *Semiconductor Lasers and Heterjunction LEDs*, Academic Press, New York, 1977.

[Kroe84] H. Kroemer, J. Vac. Sci. Technol. B, vol. 2, pp. 433-439, 1984.

[Lass91] H. E. R. Lassiter, Laser Focus World, vol. 27, pp.101-113, 1991.

[Lent90] W. Lenth, IEEE LEOS Annual Conference, Plenary Session, Boston, Mass., Nov. 4, 1990.

[Li90] K. Li, H. C. Lee, P. J. Benguhe, and M. Hirsch, Lasers and Optronics, vol. 9. pp. 28-39, 1990.

[Luo90] H. J. Luo, and P. S. Zory, IEEE Photonics Technol. Lett. vol. 2, pp. 614-616, 1990.

[McCa90] J. O. McCalsin, J. Vac. Sci. Technol. A, vol. 8, pp. 1199-1193, 1990.

[Nag80] B. R. Nag, *Electron Transport in Compoumd Semiconductors*, Springer-Verlag, Berlin, 1980.

[Park90a] R. M. Park, C. M. Rouleau, and M. B. Troffer, J. Mater. Res. vol. 5, pp. 475-477, 1990.

[Park90b] R. M. Park, M. B. Troffer, C. M. Rouleau, J. M. DePuydt, and M. A. Haase, Appl. Phys. Lett., vol. 57, pp. 2127-2129, 1990.

[Phil63] H. R. Phillip and H. Ehrenreich, Phys. Rev., vol. 129, pp. 1550-1560, 1963.

[Ren90] J. Ren, K. A. Bowers, V. Sneed, D. L. Dreifus, J. W. Cood, Jr., J. F. Schetzina, and R. M. Kolbas, Appl. Phys. Lett., vol. 57, pp. 1901-1903, 1990.

[Reyn89] R. A. Reynolds, J. Vac. Sci. Technol. A, vol. 7, pp.269-270, 1989.

[Shak73] K. L. Shaklee, R. E. Nahory, and R. F. Leheny, J. Luminescence, vol. 7, pp. 284-309, 1973.

[Shea77] D. C. O'Shea, W. R. Callen, and W. T. Rhodes, *Introduction to Lasers and Their Applications,* Addison-Wesley, Reading, Mass., 1977.

[Stre82] W. Strifer, R. D. Burhan, and D. R. Scifres, IEEE J. Quantum Electron., vol. QE-18, pp. 856-864, 1982.

[Suem89] I. Sumune, K. Yamada, H. Masato, Y. Kan, and M. Yamanishi, Appl. Phys. Lett., vol. 54, pp. 981-983, 1989.

[Sze81] S. M. Sze, *Physics of Semiconductor Devices*, John Wiley and Sons, New York, 1981.

[Thom82] G. H. B. Thompson, *Physics of Semiconductor Laser Devices*, Wiley, New York, 1980.

[Verd81] J. T. Verdeyen, *Laser Electronics,* Prentice-Hall, Englewood Cliffs, N.J., 1981.

[Ves85] S. Ves, K. Strossenger, N. E. Christensen, C. K. Kim, and M. Cardona, Solid State Comm., vol. 56, pp. 479-483, 1985.

[Wagn88] D. K. Wagner, R. G. Water, P. L. Thanyi, D. S. Hill, A. J. Roza, H. J. Vollmer, and M. M. Leopold, IEEE J. Quantum Electron. vol. 24, pp. 1258-1265, 1988.

[Wang81] C. S. Wang and B. M. Klein, Phys. Rev. B, vol. 24, pp. 3417-3428, 1981.

[Zmud90] C. A. Zmudzinski, Y. Guan, and P. S. Zory, IEEE Photonics Technol. Lett. vol. 2, pp. 94-96, 1990.

BIOGRAPHICAL SKETCH

Yu Guan was born in Beijing, the People's Republic of China in 1962. He received the B.S. degree in electrical engineering from Tsinghua University, Beijing, China, in 1985 and the M.S. degree in Physics from the University of Alabama in 1988.

In 1984, he was involved in developing optical aligning machines for photolithography at the Institute of Optical and Fine Machinery of the Chinese Academy of Sciences, Shanghai, China. Between 1984 and 1985, he worked on a CCD imaging system for laser output measurement, which was his B.S.E.E. thesis project. In July 1985, he became a graduate student in the Department of Electrical Engineering of Tsinghua University, working on an intelligent cardiogram system. In July 1986, he came to the United States to study toward his M.S. degree at the University of Alabama. His master's thesis project was on tunable CH_3F far infrared Raman lasers pumped by a high pressure CO_2 laser. He also taught physics and astronomy during his graduate studies at Alabama. Since August 1988, he has been pursuing his Ph.D. degree in electrical engineering in the photonics research group at the University of Florida. His current research area involves the development of semiconductor blue light emitting devices, especially ZnSe lasers. He is a member of the Laser and Electro-Optical Society of IEEE.

I certify that I have read this study and that in my opinion it conforms to acceptable standards of scholarly presentation and is fully adequate, in scope and quality, as a dissertation for the degree of Doctor of Philosophy.

Peter S. Zory, Chairman
Professor of Electrical Engineering

I certify that I have read this study and that in my opinion it conforms to acceptable standards of scholarly presentation and is fully adequate, in scope and quality, as a dissertation for the degree of Doctor of Philosophy.

Sheng S. Li
Professor of Electrical Engineering

I certify that I have read this study and that in my opinion it conforms to acceptable standards of scholarly presentation and is fully adequate, in scope and quality, as a dissertation for the degree of Doctor of Philosophy.

Ramakant Srivastava
Professor of Electrical Engineering

I certify that I have read this study and that in my opinion it conforms to acceptable standards of scholarly presentation and is fully adequate, in scope and quality, as a dissertation for the degree of Doctor of Philosophy.

C. K. Peng
Assistant Professor of Electrical Engineering

I certify that I have read this study and that in my opinion it conforms to acceptable standards of scholarly presentation and is fully adequate, in scope and quality, as a dissertation for the degree of Doctor of Philosophy.

Robert M. Park
Associate Professor of Materials Science and Engineering

This dissertation was submitted to the Graduate Faculty of the College of Engineering and to the Graduate School and was accepted as partial fulfillment of the requirements for the degree of Doctor of Philosophy.

May 1991

for Winfred M. Phillips
Dean, College of Engineering

Madelyn M. Lockhart
Dean, Graduate School